ALMA MATER STUDIORUM
UNIVERSITY OF BOLOGNA

SCHOOL OF SCIENCE

Laurea Magistrale in Analisi e Gestione dell'Ambiente
Curriculum in Water and Coastal Management

Geomorphological and statistical analysis of the dune changes in Lido di Classe (Ravenna, Italy) based on remote sensing techniques

Thesis in: Advanced technologies and Decision Support Systems in water and coastal management

Supervisor:
Dr. Beatrice M.S. Giambastiani

Presented by:
Regine Anne Faelga

Co-supervisor:
Dr. Luigi Cantelli
Dr. Sonia Silvestri

Unique session Academic year 2021 - 2022

Table of Contents

List of Figures

List of Tables

List of Equations

Summary

Coastal dunes are well-known for their significance in providing vital ecosystem services. However, its highly dynamic nature and its exposure to climatic and anthropogenic pressures make them one of the most vulnerable geologic features along the coastal zones worldwide. On a local perspective, the coast of Ravenna – a low-lying coastal zone located along the Northern Adriatic Sea in Italy, is among the areas that are subjected to increasing environmental risks such as coastal erosion, storm surge, groundwater and soil salinization. Restoration initiatives have been implemented in some of the protected dune areas to combat against impending risks.

This thesis aimed to contribute to the assessment of the dune restoration project in the protected natural area of the Bevano River mouth in Ravenna using UAV monitoring surveys from 2016 to 2021. The restoration measure included two windbreak wooden fences that were installed in front of the dune foot and parallel to the coast to stop wind and facilitate sand deposition and accumulation. Primarily, the objective is to assess the impact of the 2016 restoration project in the dune development in terms of sand volume changes by utilizing the Structure from Motion (SfM) photogrammetry and the Geomorphic Change Detection (GCD) toolset. Next is to establish a systematic workflow for UAV data processing and elevation data analysis that is suitable for sediment volume calculations. Last is to explore the utility of orthomosaic images for vegetation change detection in order to determine other contributing factors to the overall geomorphology of the dune ridge.

For the methodology, the UAV topographic survey, coupled with GPS ground survey using Real-time Kinematic (RTK) positioning, were carried out from 2016 to 2021 in order to assess the geomorphological evolution of the area over time. SfM photogrammetry was utilized to generate and classify the point cloud and orthomosaic images for each survey year using Agisoft Metashape Professional. The classified ground points were interpolated in ArcMap to create Digital Elevation Models (DEMs), while the orthomosaic images were utilized to confirm the possible sources of data noise in the model and assess vegetation changes. GPS points and profiles were used to validate the elevation models.

The volumetric changes in sediment storage and error analysis were calculated using the DEM of Difference (DoD) approach under the Geomorphic Change Detection

(GCD) extension toolbar in ArcMap. The results show that sand accumulation was observed along the dune foot where the wood fences were established. The following changes have also been observed - progradation of the front dune, development of insipient dunes, decrease in slope stoss, decrease of blowout features due to increase in vegetation colonization. There is also an increase in vegetation and debris cover within and near the wood fences.

Overall, it can be concluded that the windbreak fence has proven to be an effective intervention to prevent dune erosion since significant geomorphological changes and vegetation colonization have occurred based on the comparison between the 2016 and 2021 data. This is despite numerous factors affecting the overall sediment budget dynamics in the study area. The GCD toolset can be an effective monitoring tool for coastal dunes provided that the sources of uncertainties are well accounted for.

In a coastal management perspective, the results of this thesis can supplement in showcasing the importance of implementing sand trapping fences and limiting debris cleaning as nature-based solutions to combat dune degradation along the coastal zones of Ravenna. The proposed systematic workflow in this research can also be explored in creating transferable guidelines to relevant stakeholders in implementing its integrated coastal zone management (ICZM).

The manuscript has a total of five (5) chapters. Chapter one includes a comprehensive literature review on the basic principles relevant to coastal dune geomorphology and the gaps that this study would like to fill in. It also includes the information about the scope and area of the research. Chapter two provides the in-depth details about the methodology of the study that includes the data acquisition and processes, the implemented workflow for SfM, DEM creation, quality check and assessment, and vegetation analysis using the high-resolution orthomosaic images. All the results are presented in Chapter three, while the detailed discussions are in Chapter four. Conclusions and recommendations are presented in Chapter five.

Acknowledgement

Acknowledgement is duly given to my supervisor, Prof. Beatrice Maria Sole Giambastiani and co-supervisors, Prof. Luigi Cantelli and Prof. Sonia Silvestri for providing guidance, support, and the core scientific and technical concepts that are crucial to make this study possible. I would also like to thank Prof. Claudia Romagnoli for accepting the invitation to be part of my thesis panel as a co-examiner.

Acknowledgement is also given to the Integrated Geoscience Research Group (IGRG) and the Biological, Geological, and Environmental Sciences Department (BiGeA) under the Environmental Science Department of the University of Bologna in Ravenna for providing all the relevant data, resources, and assistance for the fieldwork surveys. I would also like to thank the Water and Coastal Management (WACOMA) and the Erasmus Mundus Joint Master's Degree (EMJMD) programs for giving me the opportunity to study in Europe and to widen my research career in the field of coastal management. Rest assured that all that I have learned in the program would be put into practice and of use.

Last but not least, I would like to thank not just my family in the Philippines, but also my family here in Italy for being my home away from home. I was able to survive the storms of life and the recent pandemic because they stood as my rock and my support system all throughout this journey. *Maraming salamat.*

Chapter 1. Introduction

Coastal sand dunes are important resources that are known to provide numerous ecosystem services varying from flood protection, salinization prevention, groundwater storage, to recreation and species habitat. Primarily, this ecosystem is crucial in the sediment supply for the dune-beach system (Fabbri et al., 2021; Martinez et al., 2008). Several studies on coastal dunes have been conducted over the years given its importance on human well-being and its hold on high biodiversity value (Van der Biest et al., 2017).

These aeolian landforms develop in coastal zones where there is sufficient sediment supply that can be transported inland by wind (Fabbri et al., 2017). Its size, evolution, and morphology are primarily driven by the complex interaction of different other factors including the controlling winds and the geomorphology of the nearshore and beach environment (Sloss et al., 2012). Vegetation also plays an important role in dune geomorphology dynamics as it aids in sand trapping and stabilization (Lalimi et al., 2017).

These landforms are known for their significance in providing vital ecosystem services. However, its highly dynamic nature, along with additional climatic and anthropogenic pressures, make them one of the most vulnerable geologic features along the coastal zones worldwide. Sustainable management has become a buzzword in the field of coastal management in recent years.

The interaction complexities between all the factors involved in coastal dune morphology dynamics post a huge challenge in understanding and identification of its overall sediment budget (Fabbri et al., 2017). It has been identified that regular monitoring campaigns are recommended in order to assess its dynamics and development in a quantitative manner. Over the years, close-range remote sensing platforms such as UAS and SfM photogrammetry have been integral tools to rapidly acquire and model elevation data for coastal landscape analysis (Hilgendorf et al., 2021). Open-source GIS tool sets such as the GCD have also been available to conduct volume calculations using the derived elevation models from SfM photogrammetry.

This chapter tries to synthesize relevant literature about coastal dunes, its management and monitoring within the ten (10) tenets of sustainable environmental management by Barnard and Elliot (2015), with the focus on dune fencing as a restoration tool and remote sensing as a monitoring tool. The trends in the field of dune geomorphology are also discussed to understand how and where this study can contribute and to be of added value. This chapter also includes information on the scope of the study and the characterization of the study area.

1.1. Scope of the research

The coast of Ravenna located along the Northern Adriatic Sea in Italy (Figure 1) is characterized as a low-lying coastal zone that is subjected to increasing environmental risks such as coastal erosion, storm surge, groundwater, and soil salinization. Several restoration initiatives with corresponding monitoring campaigns have been implemented in some of the protected dune areas to combat against impending risks. Biotic and abiotic processes, interactions, and feedbacks in beach-dune systems are complex and may occur at different temporal and spatial scales; hence, it is imperative to assess morphological changes and vegetation dynamics (Laporte-Fauret et al., 2021). The primary goal of the thesis is to contribute to the assessment of the dune restoration project in the protected natural area of the Bevano River mouth in Ravenna using the existing UAV monitoring surveys from 2016 to 2021. The impact of the 2016 restoration project in the dune development is evaluated in terms of sand volume changes by utilizing the SfM photogrammetry and GCD toolset. Second goal is to establish a systematic workflow for UAV data processing and elevation data analysis that is suitable for sediment volume calculations. Last is to explore the utility of orthomosaic images for vegetation change detection in order to determine other contributing factors to the overall morphology of the dune ridge.

1.2. The ten tenets of sustainable management and coastal dune restoration

According to the World Commission on Environment and Development (1987), sustainability is defined as a kind of development wherein the needs of the present are met without compromising the ability of the future generations to meet its own needs. This definition, together with the first article of the Rio Declaration, which states that humans are the center of concerns for sustainable development and are entitled to a

healthy and productive life in harmony with nature, were adapted by Barnard and Elliot (2015) in defining the tenets of sustainable management. These are principles that can be used as metrics to assess and quantify sustainability measures in the environment within the framework of the Drivers, Activities, Pressures, State, Impacts, Responses, and Measures commonly known as DAPSI(W)R(M) - a modified form of the Drivers, Pressures, State, Impact, and Response (DPSIR) model of Atkins et al. (2011). The ten tenets are the following - environmental management should be ecologically sustainable, technologically feasible, economically viable, socially desirable, ethically defensive, culturally inclusive, legally permissible, administratively achievable, effectively communicable, and politically expedient (Barnard and Elliot, 2015).

The 2013 to 2016 RIGED-RA coastal dune restoration and management project along the Ravenna coast implemented a multidisciplinary approach, wherein expertise from different fields of research were tapped to come up with an integrated and quantitative assessment in identifying restoration sites in the area (Giambastiani et al., 2016). Guidelines for coastal management and planning were also provided to aid in defining the appropriate intervention strategies for dune protection and restoration. The project concluded with the establishment of a windbreak fence along a portion of the Ravenna coast.

The restoration project implemented an Integrated Coastal Zone Management (ICZM) approach comparable to the tenets of sustainable management. Its compliance to the tenets can be assessed according to the final output and guidelines that were established from the project. In order to determine the degree of compliance of dune fencing and its monitoring to sustainable management, supporting literature will be discussed according to the different tenets. In this discussion, the activity and/ or development pressure is the dune fence establishment, and the management measure or response is the dune evolution monitoring using remote sensing and photogrammetry modeling techniques.

1.3. Dune geomorphological evolution

According to the New Jersey Administrative Code definition that was adopted in the study of Wooton et al. (2016), coastal sand dunes are defined as:

> "... wind or wave deposited or man-made formation of sand (mound or ridge), that lies generally parallel to, and landward of the beach and the foot of the most

inland dune slope. “Dune” includes the foredune, secondary or tertiary dune ridges and mounds, and all landward dune ridges and mounds, as well as man-made dunes, where they exist.”

Coastal dunes are highly dynamic systems both in the temporal and spatial context as they immediately respond to marine, aeolian, biological, and anthropological processes when subjected (Wooton et al., 2016; Bird, 2011; Davidson-Arnott, 2019; Maun, 2009; Garcia-Lozano et al., 2020). The temporal dependence of the beach-dune dynamics starts when storm waves and swash erode, wash over, wash through or totally destroy dunes and supply sediment to the beach and nearshore (Carter and Stone, 1989; Sallenger, 2000; Jackson and Nordstrom, 2020). Backshore and dune recovery occurs during onshore sediment transport, wherein a buffer against erosion is created for onshore winds to blow sand into the dune. Essentially, the erosional phase of the coastal dune change is wave-induced while the depositional phase is wind-induced but overall, dune and beaches are spatially within the same sediment exchange system (Jackson and Nordstrom, 2020). Hence, the sediment contribution from the nearshore to the dunes is vital, as well as the accretion rates in the foredune as it corresponds to volume supply to the beach over the long term (Aagraad et al., 2004). Sand deposition is also facilitated by the presence of tolerant vegetation that later on increases the stabilization and growth of the dune system (Laporte-Fauret et al., 2021; Wooton et al., 2016).

Dune erosion and coastal flooding are driven by the maximum storm surge and of breaking waves, wherein the coastal dune system response is dependent on the total water elevation relative to the dune or berm height together with other morphological factors of the dune field, its distance from the sea and its sedimentary characteristics (Edelman, 1972; van de Graaff, 1977; Stockdon et al., 2007; Overton et al., 1994; Fernández-Montblanc et al., 2020).

Episodic events such as coastal storms, in addition to drivers associated with climate change such as sea level rise, have a direct impact on coastal zones too (Fernández-Montblanc et al., 2020). Aside from the climatic aspect, anthropogenic pressures such as tourism activities and rapid urbanization along coastlines also affect the dynamics of coastal dunes. It is now recognized that coastline changes and human activities are mutually linked (Gopalakrishnan et al., 2011; Lazarus et al., 2011, 2016;

Murray et al., 2013; Jackson and Nordstrom, 2020). Hence, coastal zones in general can be considered climate change hotspots (Wong et al., 2014; Sekovski et al., 2020).

1.4. Dune fencing as coastal dune management

The global concerns on climate change impacts have led to research focus on the processes and morphologic response of coastal systems in order to implement management strategies to protect these highly dynamic and vulnerable systems. Proper mitigation strategies and adaptation measures are integral tasks for coastal managers in order to reduce the risk to extreme events (IPCC, 2014). Management in relation to dune systems is done by implementing strategies to either protect, conserve, preserve or restore its natural value and the local communities against the effects of dune system changes (Labuz, 2015).

However, early coastal developments have been more on hard-infrastructure construction that are either for protection or for tourism purposes. The lack of integrated management solutions has led to the accelerated degradation of the natural beach and dune systems worldwide (Jackson and Nordstrom, 2020; Alonso et al., 2002; Nordstrom, 2008; Pilkey et al., 2011; Sarda et al., 2013; Taylor et al., 2015; Garcia-Lozano et al., 2020).

Environmental regulations are enforced worldwide to combat further degradation. In Europe, several European legislations, and networks such as the Habitats Directive and Natura 2000 have been established to transpose EU directives into national legislation (Esteves, 2014). In the case of Natura 2000, the national government should take all the necessary protection measures of the habitat and species in the identified sites, which usually includes coastal dunes. Several literatures have accounted that the European coastal foredunes have been stabilized by reprofiling, planting vegetation and dune fencing, and/or beach nourishment (Matias et al., 2005; Nordstrom and Arens, 1998; Arens et al., 2001; Ruz and Anthony, 2008; De Vriend and Van Koningsveld, 2012) over the past century (Laporte-Fauret et al., 2021). Soft or limited engineering, along with Nature-Based Solutions (NBS) and even de-engineering efforts have been among the preferred intervention solutions for coastal zones as they enable a more dynamic evolution and functioning. Soft engineering schemes include beach nourishment, dune fencing for restoration and managed realignment (Esteves, 2014). Dune fencing that can promote vegetation growth have

been widely used given their relatively lower cost and maintenance compared to sand nourishment. In addition, the fences are useful for long duration rehabilitation programs (NSW DLWC, 2001). The materials used in the fence establishment are durable and not easily biodegradable, making it a good alternative to hard-structure engineering (Mascarenhas, 2009).

The positive effect of the sand trapping fences is due to the local reduction of wind velocity that leads to downwind sediment accumulation and later initiates dune stability (Eichmanns et al., 2021). Knowledge of the beach-dune system interaction is vital in identifying suitable sites for the installation of these fences. Usage of fences is considered for environmentally and culturally sensitive areas where use of heavy equipment is not possible and public access is limited (NSW DLWC, 2001).

The effectiveness of dune fencing in increasing sediment accumulation have been evaluated in several studies that were mentioned in the works of Jackson and Nordstrom (2020) (e.g., Savage, 1963; CERC, 1984; Hotta et al., 1987, 1991; Miller et al., 2001; Anthony et al., 2007) and Eichmanns et al. (2021) (e.g., Eichmanns and Schüttrumpf, 2020 & 2021; Itzkin et al., 2020; Ruz and Anthony, 2008). Aside from fences to mimic natural dune formation, it can also aid in controlling foot access and against unwanted anthropogenic activities. Countries like the USA (e.g., Mendelssohn et al., 1991; Daley et al., 2000; Herrington, 2004; Martinez et al., 2006), France (Roze and Lemauviel, 2004) and Portugal (Dias et al., 2003; Matias et al., 2005) have adapted dune fencing measures as mentioned in the work of Mascarenhas (2009). Fence installation for dune restoration has also been implemented along the Adriatic Coast in Emilia-Romagna, Italy (e.g., Giambastiani et al., 2016; Fabbri et al., 2017 & 2021).

The emergence of soft-engineering solutions to coastal dune restoration can be considered highly compliant in all the ten tenets. Although it may be susceptible to vandalism and material degradation over time, its relatively low-cost and simple method to induce sand accretion make it ecologically sustainable, technologically feasible and economically viable. The straightforward and less-invasive build of these fences compared to hard structures makes it compliant to the remaining tenets. However, the solution still requires evaluation on its efficacy in the increase of sediment accumulation and its impact on the overall sediment balance. Agreeing to Jackson and Nordstrom (2020), the evaluation for sustainability should not only be limited to the effects of the

dune fences as a built project itself, but rather include projections and efficacy of these measures as an alternative for adaptive management through monitoring.

1.5. Coastal dunes monitoring using Remote Sensing

Aeolian sand dune research has been around since the 1960s and the availability of advanced instruments, development of more comprehensive models, and increase in recorded publications have demonstrated its increasing pace through time (Thomas and Wiggs, 2008; Livingstone et al., 2007; Stout et al., 2009; Zheng et al., 2022). Literature over the years have also proven the advances of coastal dune geomorphology studies through remote sensing in terms of mapping its extents, quantification and monitoring of its patterns and dynamics (Zheng et al., 2022). The advent of high-resolution data for surface topography characterization has led into the development of geomorphology as a quantitative science (Kasprak et al., 2019). Several remote sensing techniques such as Terrestrial Laser Scanning (TLS), aerial Light Detection and Ranging (LiDAR), and Unmanned Aerial Survey (UAS) have enabled geomorphologists to access fundamental insights into landscape evolution since the derived point clouds can be used to produce high-accuracy Digital Elevation Models (DEMs) that enable deeper understanding into geomorphic change and quantification of a number of metrics that are important to landscape management and restoration for coastal system processes (Zheng et al., 2022; Kasprak et al., 2019). The advances in ground-based and remotely based surveying technologies enabled the availability of high-resolution repeat topographic surveys, which have been widely used in the field of earth science (Passalacqua et al., 2015; Wheaton et al., 2009a). In addition, the advances over the years have made geomorphic change monitoring and sediment budget estimation a tractable approach for monitoring applications both in research and practice (Wheaton et al., 2009a).

Among these terrestrial and aerial survey methods, UAS platforms have been utilized further for dune monitoring given its affordability and user-friendly interface compared to its other surveying counterparts. Surface topographic surveys at high spatial and temporal resolutions along coasts are possible using UAS and Structure from Motion (SfM) photogrammetry. SfM photogrammetry is based on a structured acquisition of images that is used to reconstruct 3D scene geometry and camera motion based on a new generation of automated image-matching algorithms (Mancini

et al., 2013). Both the UAS platforms and SfM photogrammetry have shown widespread advancement in the last decade (Anderson et al., 2019; James et al., 2019; Hilgendorf et al., 2021). DEMs built from UAS surveys can be used to produce DEM of Difference (DoD) maps to estimate the net change in storage for morphological sediment budgets (Church and Ashmore, 1998; Wheaton et al., 2009a). Several authors have already proven the reliability of the DSM or DEM that were obtained from UAV-SfM on various natural environments. There are different tonal contrasts between tidal flats, beaches, and dune systems. However, there is still a need to assess the accuracy of point clouds and surface models derived from UAS on sandy coastal environments (Mancini et al., 2013).

DoD or Geomorphic Change Detection (GCD) is a useful geomorphology tool developed by the Riverscapes Consortium using the methodology of Wheaton et al. (2009a), Wheaton (2008) and Wheaton et al. (2009b). It can provide information about the extent, magnitude and landscape form changes that occur within an inter-survey period to understand the overall sediment budget of the area of interest or the spatial distribution changes of sediments through time (Grams et al., 2015; Collins et al., 2016; Sankey et al., 2016). Hence, landscape change can readily be characterized by contrasting repeat topographic surveys.

The model reconstruction from SfM photogrammetry has to be validated and error analysis has to be performed to ensure the reliability of the change detection result of the GCD. According to Wheaton et al. (2019a), uncertainty in GCD modeling on morphology has already been assessed in various studies (e.g. Lane et al., 1994; Milne and Sear, 1997; Brasington et al., 2000; Lane, 1998; Lane et al., 2003) as data and model uncertainties render the GCD result prone to misinterpretation.

In Italy, seasonal coastal changes were monitored using high-accuracy and quality photogrammetry images from unmanned aerial vehicles (UAV) in the work of Scarelli et al. (2017). The performance of these methodologies was assessed, and the model outputs were recommended to be utilized in other disciplines to aid in the application of the ICZM in the Emilia-Romagna coasts. Geomorphological analysis has also been performed in the study of Fabbri et al. (2017), wherein foredune ridges along the Ravenna coast of Emilia-Romagna were surveyed and assessed using TLS technology. A recent study conducted by Fabbri et al. (2021) has investigated the

vegetation and geomorphological changes on a dune field restoration site in Punta Marina in Ravenna using UAV and SfM photogrammetry. However, the study utilized a different evaluation approach, which was the Digital Shoreline Analysis System (DSAS) freeware of the United States Geological Survey (USGS) instead of GCD. Other analysis approaches have been done in different coastal studies within the Adriatic coast and its coastal dunes, but nonetheless, all with the same goal to aid in the overall integrated coastal management of the area (e.g., Sekovski et al., 2020; Fernandez-Montblanc et al., 2020; Taramelli et al., 2015).

Fragmentation and conflicts between different levels of government is said to have been an issue of coastal management in Italy (Airoldi et al., 2015). In the past, the conflicting interests between economic and environmental valuations had an impact in the degradation of coastal resources – including natural dunes. Hence, the implementation of dune restoration efforts along the region can mitigate further degradation and understanding the system change through monitoring programs over seasonal timescales is important as it can support the establishment of new guidelines for coastal system protection (Scarelli et al., 2017). The availability and continuous advancement of remote sensing, specifically UAS and SfM photogrammetry, is an advantage that must be utilized, especially within the Emilia-Romagna coasts given their highly dynamic and vulnerable nature.

Remote sensing for coastal studies has been evident over the past 20 years and its momentum of use has increased and has been apparent based on a number of published literatures. UAS coupled with ground-based GPS as a monitoring or management tool can be ascertained that it complies within the ten tenets of sustainable management. Its non-invasive nature, relative affordability, ease of use, accessibility, and scalability makes it a sustainable monitoring tool for beach-dune systems. The limit of drone use and access can easily be addressed by following the protocols set by the governing body within the area of interest. The use of UAS and SfM on dune morphodynamics in Italy is still in its infancy stage. Therefore, continuous progress and algorithm improvement to quantify dune interaction using remote sensing techniques is still essential.

1.6. Study site characterization

The Emilia-Romagna coast (Figure 1) is a 130-kilometer coastline made up of flat alluvial sandy system that borders a portion of the north-western Adriatic Sea, between the Po Delta on the north and the Cattolica town on the south (Airoldi et al., 2015; Harley et al., 2016). The coastline consists of sandy beaches, making it famous as one of the leading beach destinations in Europe. It is an area with renowned environmental, cultural, and economic value. In terms of local hydrodynamic conditions, the region is exposed to moderate wave action, a microtidal regime of around 30 to 80 cm between neap and spring tides with powerful diurnal and semidiurnal elements (Biolchi et al., 2022). It is also subjected to oceanographic conditions such as high seasonal variability, sharp stratification, and high productivity rates (Zavatarelli et al., 1998; Airoldi et al., 2015).

There are two prevailing wind patterns known in the region – the Bora wind from north-east and the Sirocco from the south-east (Zanuttigh et al., 2015). More energetic waves, which are high, steep, and relatively short, are related to Bora wind since strong winds funnel and increase their velocity downhill off the mountainous Croatian coast. On the other hand, Sirocco produces long waves and piles up water in the northern part of the Adriatic basin (Biolchi et al., 2022). The prevalent wave direction is the Bora wind due to the orientation of the coast (Amaroli et al., 2011). Most intense storms are generated by this wind and have a very strong influence in terms of the wave climate and current circulation in the northern Adriatic (Signell et al., 2010; Amaroli et al., 2011). The winter storms brought by this wind decrease the resilience of dune systems, thereby increasing coastal vulnerability and losses in terms of environmental, social, and economic aspects (Callaghan et al., 2009; Esteves et al., 2012; Forbes et al., 2004; Scarelli et al., 2017).

Ravenna is the major coastal city of the region. It has one of the largest seaports in Italy and has been considered as the core port of the Trans European Transport Network (TEN-T) by the European Commission (Airoldi et al., 2015). Its harbor and coast are primarily made up of sandy beach with gently sloping seabed of about 6 m km^{-1} and has shallow subtidal sediments from well-sorted fine to medium sand. Aside from port activities, tourism has also been an integral economic activity in the area. Both anthropogenic and natural pressures such as coastal erosion and land

subsidence over the years have affected the coast of Ravenna. Thus, the need to install structural and non-structural defense measures such as breakwaters, groynes, and revetments to combat the area's high susceptibility to various hazards (Armaroli et al., 2009; Perini et al., 2017) has been evident since the 1970s, but at the same time, these structures have also impacted the landscape negatively. Increased sedimentation, loss of native habitats, eutrophication, and poor water quality have been observed following the installation of these structures (Airoldi et al., 2015, Preti et al., 2010; Sekovsi et al., 2020). Nature-based and soft-engineering techniques such as beach nourishment and dune fence construction have been initiated as alternative solutions to combat coastal erosion.

The Restoration and management of coastal dunes along the Ravenna coast (RIGED-RA) Project between 2013 to 2016 performed a thorough assessment of the dynamics, erosion, and vulnerability of the Northern Adriatic coast and its associated residual dunes in order to identify proper intervention for dune protection and restoration (Giambastiani et al., 2016). Towards its end in 2016, the project was able to install a set of 465 m wooden fences along a portion of the Bevano River Dune Ridge in Lido di Classe in Ravenna as shown in Figure 1.

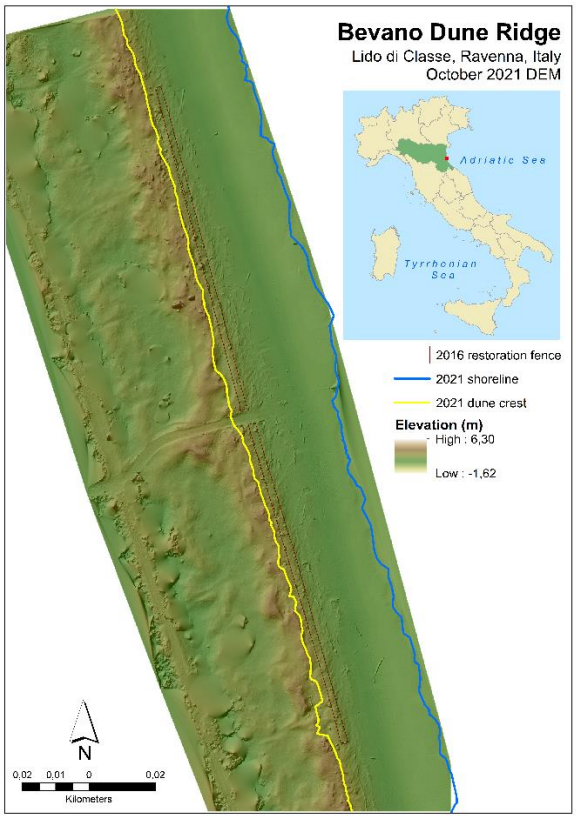

Figure 1. Location of the study area in Lido di Classe, Ravenna, Italy.

Chapter 2. Methodology

2.1. Survey data collection

Several monitoring campaigns using UAV surveys were conducted after the fence installation as shown in Table 1. The survey dataset includes UAV surveys from the I.G.R.G. (Integrated Geosciences Research Group) of the BiGeA Department (Biological, Geological, and Environmental Sciences) of the University of Bologna (UNIBO) and the fieldwork surveys during the Water and Coastal Management (WACOMA) Program under the Erasmus Mundus Joint Master's Degree (EMJMD).

SURVEY DATE	CODE	OUTPUT
28 Oct 2016	S4	GPS data of targets, point cloud, DEM, orthomosaic
08 Mar 2017	S6	GPS data of targets, point cloud, DEM, orthomosaic
04 Jul 2017	S9	point cloud, DEM, orthomosaic
15 Oct 2018	W1	GPS data of targets, GPS profiles, point cloud, DEM, orthomosaic
30 Oct 2019	W2	GPS data of targets, GPS profiles, point cloud, DEM, orthomosaic
05 Nov 2020	W3	GPS data of targets, GPS profiles, point clouds, DEM, orthomosaic
25 Oct 2021	W4	GPS data of targets, GPS profiles, point clouds, DEM, orthomosaic

Table 1. Survey information used in the study.

The details of the data acquisition and processing are shown in Table 2. GPS data points were collected using a Leica DGPS (Viva GNSS GS15 GPS) that worked with a Real Time Kinematic (RTK) system to ensure sub metric accuracy. The coordinate reference system that was used is the WGS 84/ UTM 32. The collected data points include several profile transects across the beach that were captured from the coastline to the back dune near the pine forest area and the drone targets. It is worth noting that only the surveys conducted from 2018 to 2021 have profile transect data and that the reading interval between points was set to one (1) meter.

The aerial photographs for the 3D reconstruction were captured using a DJI Phantom drone (Figure 2), with the camera technical specification in Table 2. The flight plans were defined in the UAV software and the actual data acquisitions were manually driven by a remote pilot. The flying height was set to 20 m. Targets were established on site and were geolocated using GPS (Figure 2). These targets were used to georeference the captured images for the data processing and DEM development.

UAV drone images
• 2016 to 2019 - DJI FC300X • 2020 - DJI FC300C & DJI FC300X • 2021 - DJI FC7203
GPS
• Leica DGPS (Viva GNSS GS15 GPS) • Real Time Kinematic (RTK) system
Coordinate system
• ETRS 89 UTM Zone 32N • conversion tool: ConveRgo_ge
Spatial analysis & mapping
• ArcMap 10.6.1 • QGIS Desktop 3.22.4 • Python 3.9
Structure from Motion photogrammetry
• Agisoft Metashape Professional 1.7.4 build 12898
Change Detection
• Geomorphic Change Detection (GCD) Software, Riverscapes Consortium

Table 2. Hardware and software used for the data acquisition and processing.

Figure 2. On site photos of the GPS and UAV survey at the study site on 25 October 2021.

For the GPS and UAV survey post-processing, the ellipsoidal heights were converted to geodetic height using the ConveRgo software (https://www.cisis.it/). The collected GPS points from the drone targets were used for the image alignment in the SfM photogrammetry and as the basis for the DEM validation and profile transects comparison.

2.2. SfM processing

The overall methodological framework of the study is shown in Figure 3. For the SfM processing worklow, the recommendation on the Agisoft Metashape manual was followed. However, the DEM used for the change detection analysis was processed in ArcMap 10.6.1 using the point cloud derived from the SfM processing. The workflow for SfM photogrammetry is shown in Figure 5.

From the UAV topographic survey, multiple overlapping photos were loaded in the Agisoft Metashape Pro software and initial image filtering was performed using the image quality estimation tool. In this step, the value is calculated according to the sharpness level of the most focused part of the photo. Only images with quality value of >.50 units based on the sharpness level of the most focused part of the photo were considered good quality and were retained. The initial filtering also includes removing photos from the take-off and landing of the drone. After the initial image quality check, the processing area was established using a bounding box and it was followed by the image alignment process. The values set for alignment parameters are indicated in Table 11 in the Appendix.

The alignment process includes aerial triangulation and bundle block adjustment, wherein the software searches for feature points on the images and matches them across images into tie points (Agisoft LLC, 2021). The camera position and calibration parameters for each image are also identified. Sparse point clouds and a set of camera positions are produced after the implementation of this step and are used for the depth map and 3D surface reconstruction.

The Ground Control Points (GCPs), measured by GPS, were then loaded into the program to tie the model into its accurate location on ground. A combination of manual and guided marker placement was implemented in the process. The former was done as an initial step, where individual targets were located in each of the photos and the marker was manually placed on it according to the target name as shown in Figure 4. The manual markings have then guided the software to automatically adjust the location of the remaining marking according to the GCP coordinates.

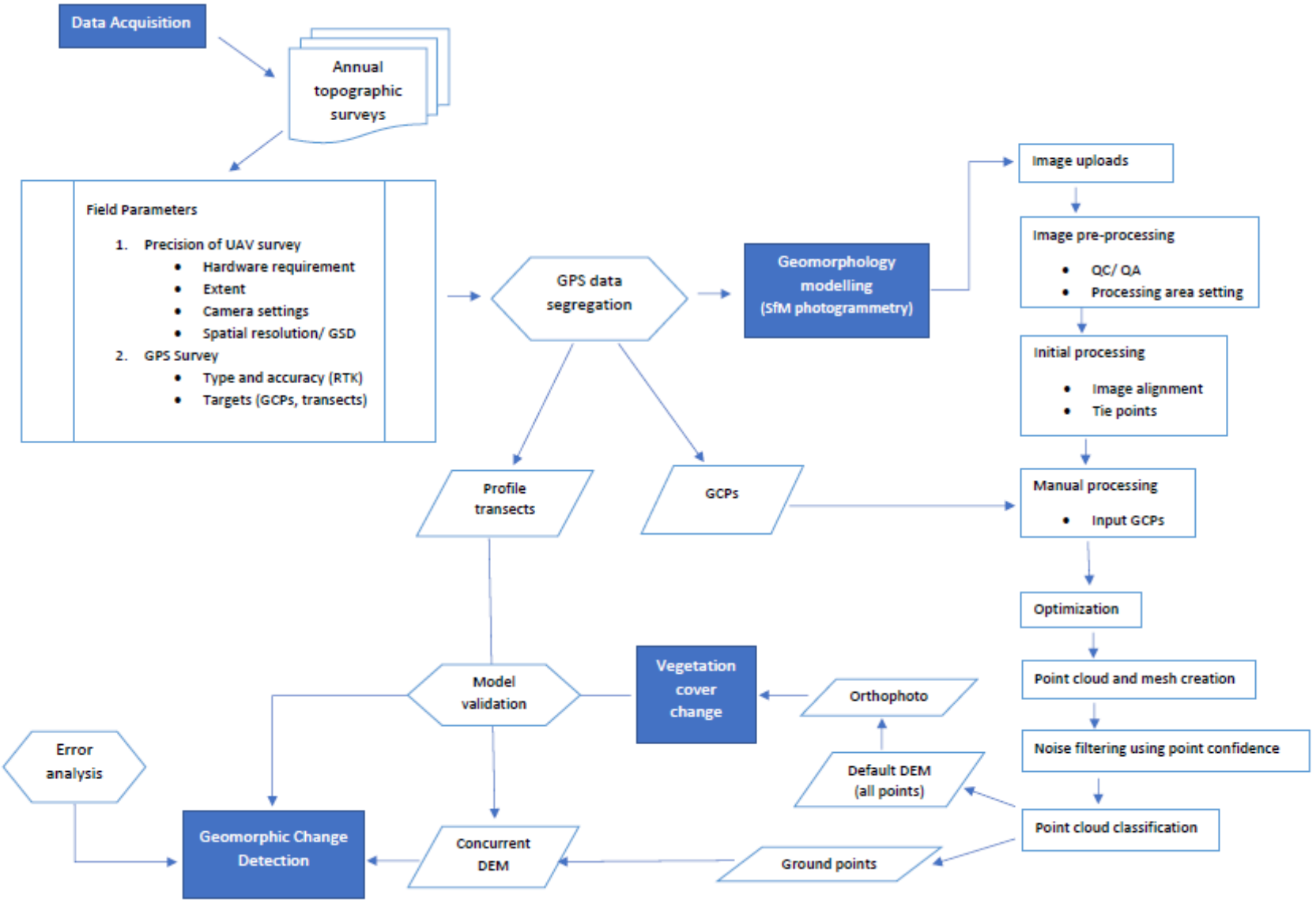

Figure 3. Methodological Framework of the study.

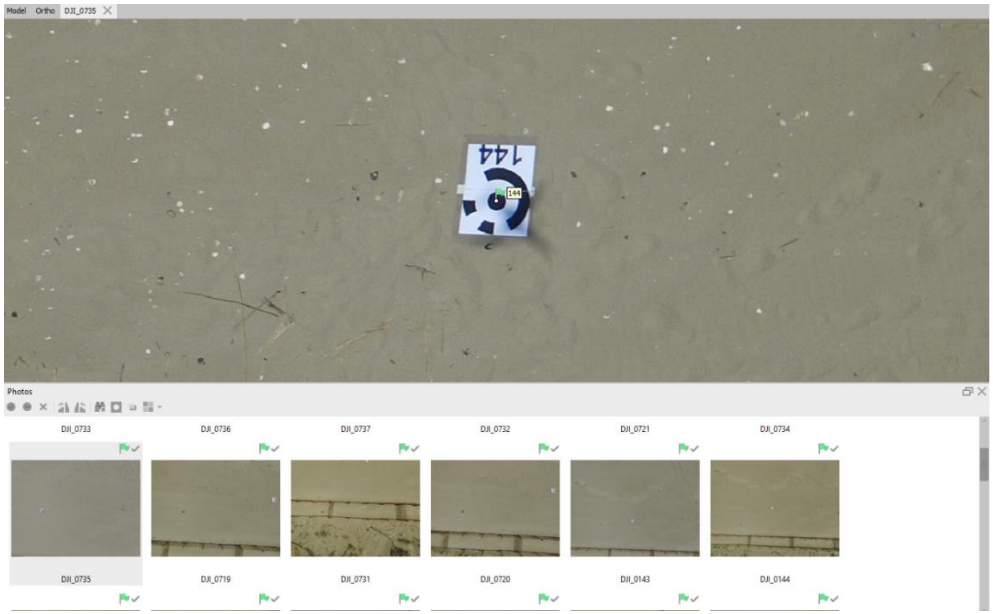

Figure 4. Manual marker placement in the aligned photos based on GCP coordinates.

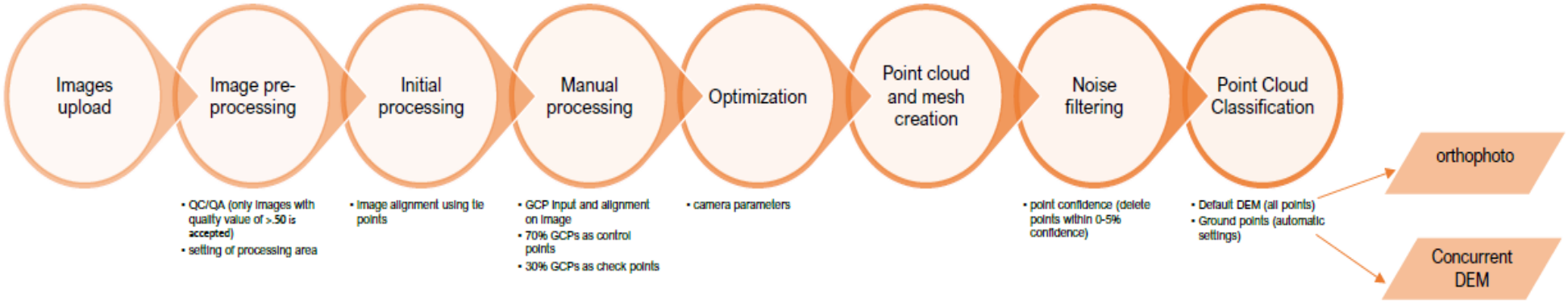

Figure 5. SfM workflow employed in the study.

After the marker placement, each GCP was assigned as either control or check points. Control points are used to reference the model while the checkpoints are used to validate the accuracy of the camera alignment and the optimization procedure results (Agisoft LLC, 2021). The 70-30 rule was implemented in selecting the control and checkpoints – 70% of the total GCPs were used as control points while 30% were used as checkpoints. After this step, optimization of the camera alignment was performed to improve the accuracy. It is based on all available measurements and corresponding accuracies – including image projections of the tie points and markers, GPS coordinates of image centers, GCP coordinates, and scale bar distances. After which, the creation of depth maps and dense point clouds were done. The values and the parameters used in the optimization process, depth maps, and point cloud generation are shown in Table 12 in the Appendix.

Noise removal was performed after the dense cloud generation. Points that are too high or low were selected and deleted to avoid spikes in the final 3D model and DEM. The filtering of points by confidence value was the primary process performed in this step. Points with confidence value from 0-5% were removed. The remaining dense point clouds were classified to automatically divide all points into two classes – ground points and the rest using the automatic classification of ground points. The parameters applied for the automatic ground points classification are listed in Table 13 in the Appendix. All classified points were used in the automatic DEM creation in the software that is used to create the orthomosaic while the classified ground points are the ones used to create the DEM for the change detection part. The details and parameters used in the DEM reconstruction, orthomosaic generation, and the overall system settings used are shown in Table 14 in the Appendix. The final output in the SfM processing was a DEM of all points, orthophotos, and dense cloud points of all the classified ground points. Same values in all the parameters were applied to all the topographic surveys to ensure coherence and comparability among the surveys. The spatial resolution of all the 3D models were set at 0.1 m x 0.1 m.

2.3. DEM validation

It is essential to determine the accuracy of the produced elevation models before using them for the geomorphology characterization. Geographic Information System (GIS), particularly ArcMap 10.6.1 and QGIS Desktop 3.22.4, and Python programming were used in the DEM validation process as shown in Figure 6.

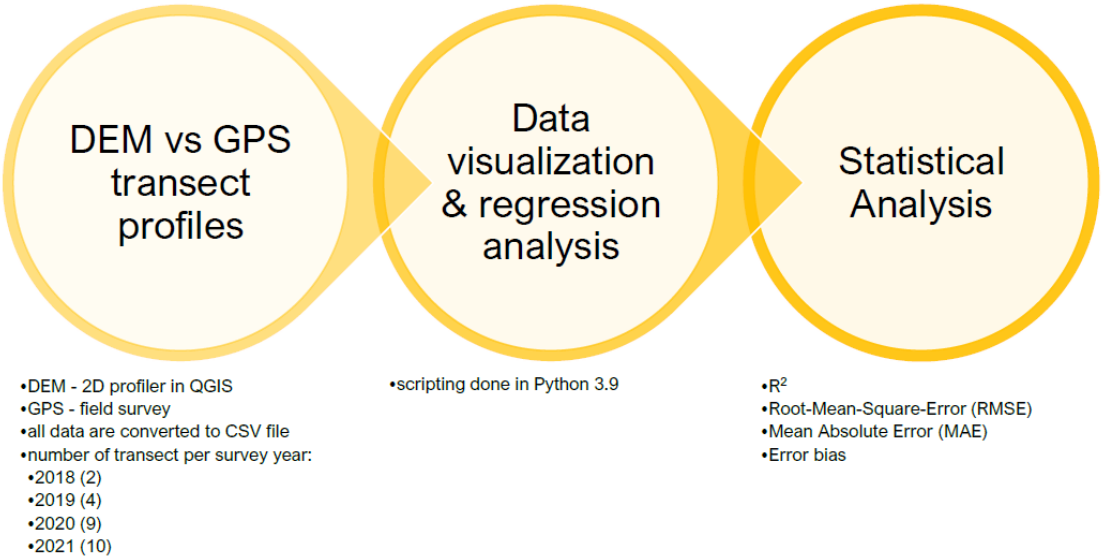

Figure 6. DEM validation processing workflow.

The 2D profiler in QGIS was used to extract the elevation values for all the survey transects. Only the October 2018 (W1), October 2019 (W2), November 2020 (W3) and October 2021 (W4) surveys have GPS transect surveys and are used in the validation process. All datasets were converted to CSV and were visualized and regressed using scripts created and ran in Python 3.9. The statistical measures used were R^2 and Root-Mean-Square-Error (RMSE) to quantify how well the regression model fits in both percentage and absolute terms. Other statistical measures were also utilized - the Mean Absolute Error (MAE) and the Mean Bias Error (MBE) or Bias. MAE represents the average of the absolute difference between the model and the actual observations in a linear score as opposed to RMSE that measures the average magnitude of errors in a quadratic scoring rule. MBE or Bias is the average error representing the systematic error of a model – in this case, if the DEM elevation values are under or over the GPS values (Kato, 2016).

2.4. Geomorphic Change Detection (GCD)

The assessment of the geomorphic change was implemented using the GCD 7 AddIn for ArcGIS 10.x toolset developed by Wheaton et al. (2009a) and the

Riverscapes Consortium (https://gcd.riverscapes.xyz/). The toolset enables users to import surface rasters that allow hillshade, slope, and error rasters generation. The DEM input in the change detection analysis is derived from the classified ground dense point cloud data that was produced in the SfM processing. An Area of Interest (AOI) that consists of the foredune to beach area was also used as the processing extent in the DEM differencing.

The error raster was created using the reported control point error values in the SfM processing as shown in Figure 7. These values are then used to determine the propagated error applied to each cell using the following equations (Lane et al., 2003):

$$\sigma_c = \sqrt{\sigma_1^2 + \sigma_2^2} \quad (1)$$

where σ_c is the root sum of square of uncertainty for each change interval; σ_1 and σ_2 are the squares of uncertainty for the older and newer time steps, and:

$$t = \frac{z_{t2} - z_{t1}}{\sigma_c} \quad (2)$$

where t is the t-statistics, z_{t2} and z_{t1} are the elevation of the raster cell for the newer (t_2) an older (t_1) time step, respectively.

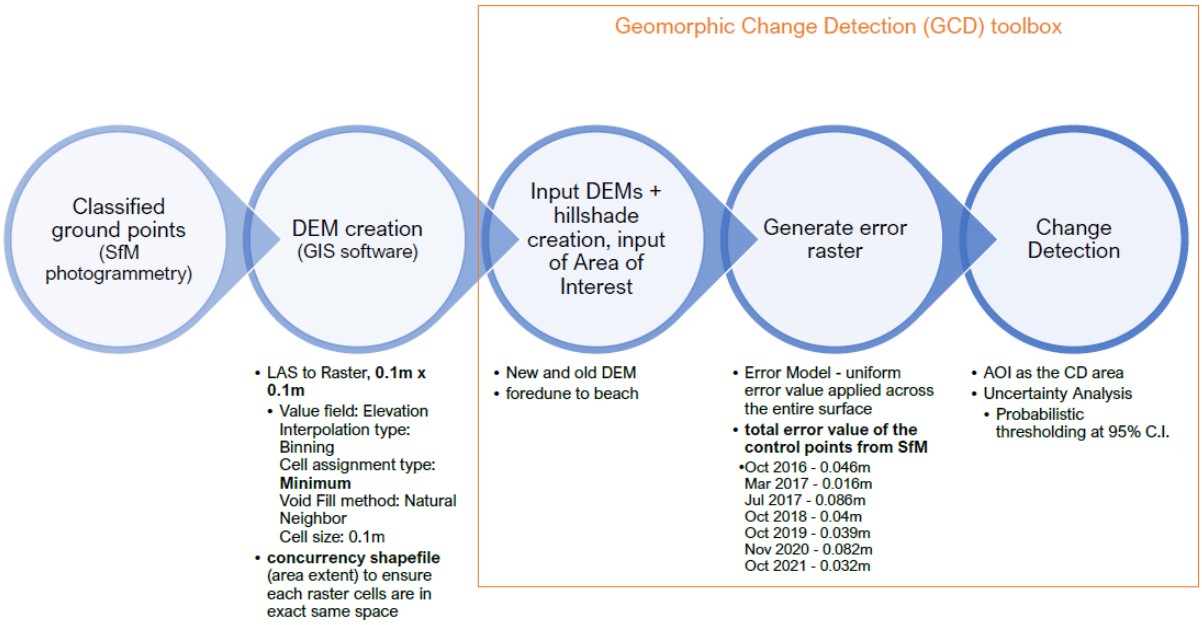

Figure 7. Geomorphic Change Detection workflow.

The T-statistics can be used as a thresholding level of significant change, where values of t > 1.96 mean confidence interval of 95% for a two-tailed t-test. The values that fall below the confidence threshold are removed from the output change raster

that improves the likelihood that a significant change was captured (Hilgendorf et al., 2021).

The method uses the difference between older DEM subtracted from a newer one to provide a spatially continuous estimate of the topographic changes within the study area (Kasprak et al., 2019). The percent sediment imbalance metric was calculated using the equation:

$$SI = \frac{(V_{DEP} - V_{EROS})}{2*(V_{DEP} + V_{EROS})} * 100 \quad (3)$$

where V_{DEP} is the volume of deposition or the positive topographic change, V_{EROS} is the volume of erosion or the negative topographic change.

This equation is applied when using the topographic change detection to characterize the sediment dynamics of an area (Wheaton et al., 2013; Kasprak et al., 2015; Kasprak et al., 2019), wherein volumes are estimated by adding the cell-by-cell depth of change multiplied by the pixel area for all the cells.

According to equation (3), an S.I. of 0% means that the erosional or depositional volumes were exactly the same. On the other hand, an S.I. value of 50% or -50% indicates a depositional or erosional topographic change.

DEM comparisons were performed to detect both annual change detection per year (2017-2016, 2018-2017, 2019-2018, 2020-2019, 2021-2020), and change across the whole period of time (2021-2016).

2.5. Vegetation cover processing

The vegetation change analysis from 2016 to 2021 was performed based on the methodology by Silvestri et al. (2022), with some modifications applied (Figure 8).

The initial step is to delineate the shoreline as the basis for the transect that will be used as the boundary condition in creating the grids. The ISO cluster unsupervised classification in ArcMap was used to distinguish between water and non-water features in the October 2021 (W4) orthomosaic. The classified features were filtered and converted from raster to polygon. The boundary between water and non-water features was used as the basis in manually delineating the shoreline.

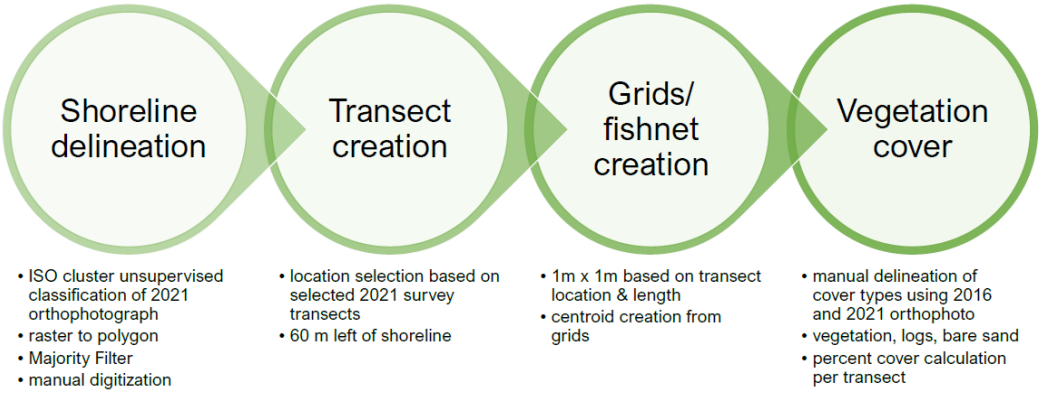

Figure 8. Vegetation analysis workflow.

Transect creation was then performed after shoreline delineation. A total of seven (7) transects 60 m long from the shoreline were drawn (Figure 9) and 1m x 1m grids were created in ArcMap. These grids were used as the input to create centroids that are used to calculate the percent cover per transect. Each centroid was manually assessed and classified according to its dominant cover feature that could either be vegetation, logs or debris, and bare sand. A simple percent cover calculation was implemented to determine the vegetation cover change from the 2016 and 2021 orthomosaic images.

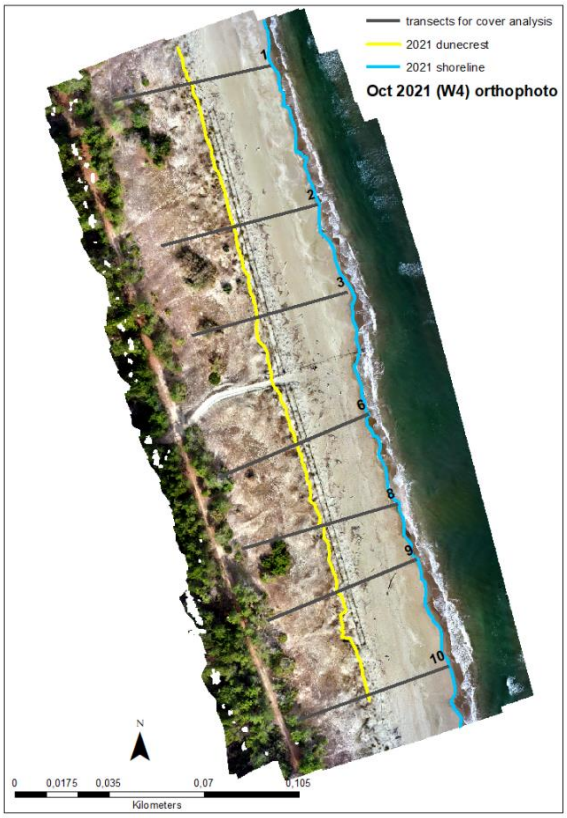

Figure 9. Location of transects for the vegetation cover analysis.

2.6. Meteo-marine data

Historical meteo-marine data has been collected to validate the change detection results. The ERA5 monthly averaged data on single levels from 1979 to present of the European Center for Medium-Range Weather Forecasts (ECMWF) was used to extract dataset such as the Mean Wave Direction (mwd), Significant Height of Combined Wind, Waves, and Swell (swh), 10m wind speed, and both the 10m u (eastern) and v (northern) component of wind. The ECMWF operates two services from the European Union's Copernicus Earth observation programme, the Copernicus Atmosphere Monitoring Service (CAMS) and the Copernicus Climate Change Service (C3S). The ERA5 data is ECMWF's fifth generation reanalysis data for the global climate and weather for the past decades. The reanalysis is a data assimilation process, where it combines model data with observations from across the world into a globally complete and consistent dataset utilizing physics laws (Hersbach et al., 2019). The ERA5 data is grid raster type with 0.5° x 0.5° or about 50 km x 50 km horizontal resolution and with a monthly temporal resolution. The spatial location of the grids is shown in Figure 10a.

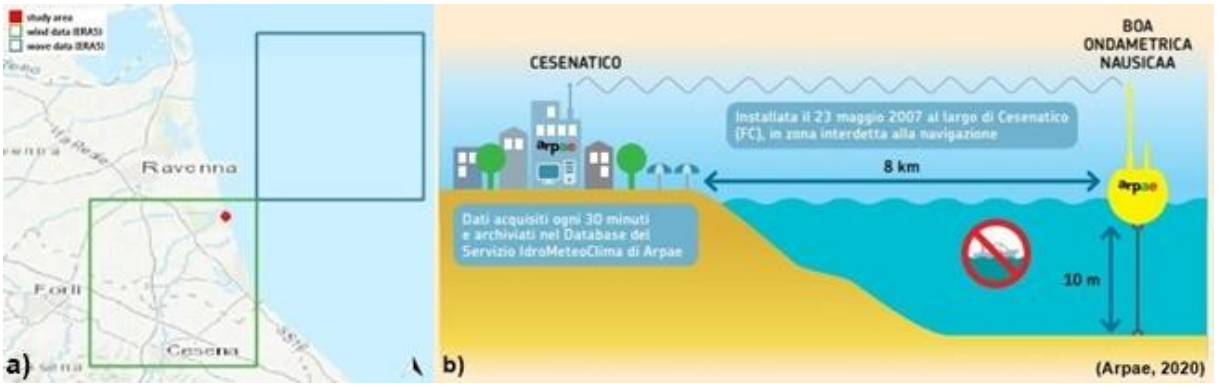

Figure 10. ERA5 grids used for the historical wave and wind data from 2016 to 2021 (a) and location of the ARPAE wave buoy in Cesenatico (b).

It should be noted that there was no ERA5 wave data that falls within the study area, so the closest grid available was utilized. Monthly data of all the parameters from 2016 to 2021 were extracted to see the overall trend and validate the erosional behavior shown in the GCD DEM differencing result. The Arpae 2020 hydro-meteo and climate report for Emilia-Romagna was utilized to supplement the wind and wave data of ERA5. The historical data from the wave buoy in Cesenatico (Figure 10b) from 2007 to 2020 was used to assess the wind and storm surge pattern over time.

Chapter 3. Results

3.1. SfM photogrammetry

DEMs and RGB orthomosaic images at 0.1 m x 0.1 m resolution are shown in Figure 11 and Figure 12, respectively. The elevation values range from -1.62 to 6.30 m.

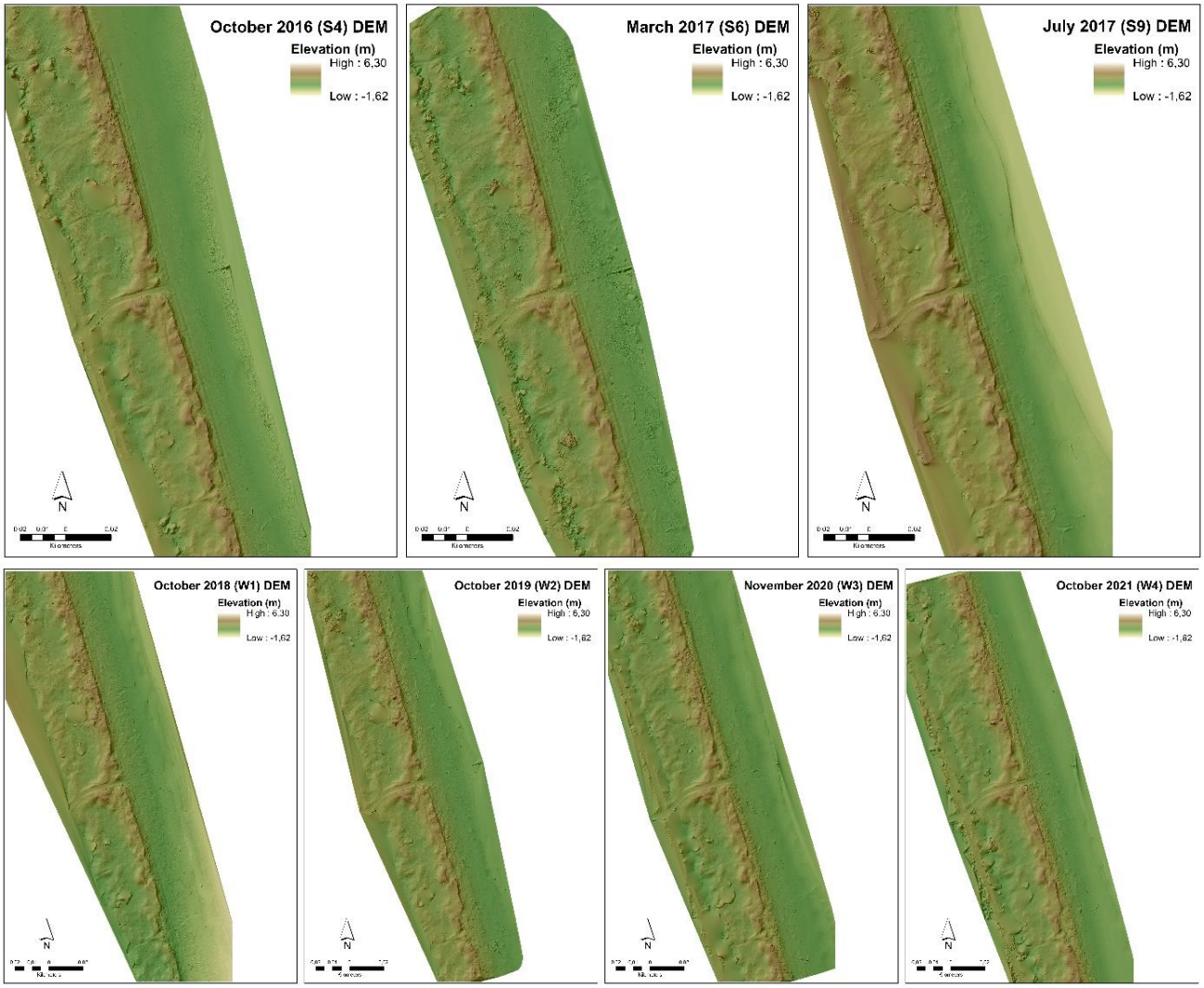

Figure 11. DEM of all the topographic surveys.

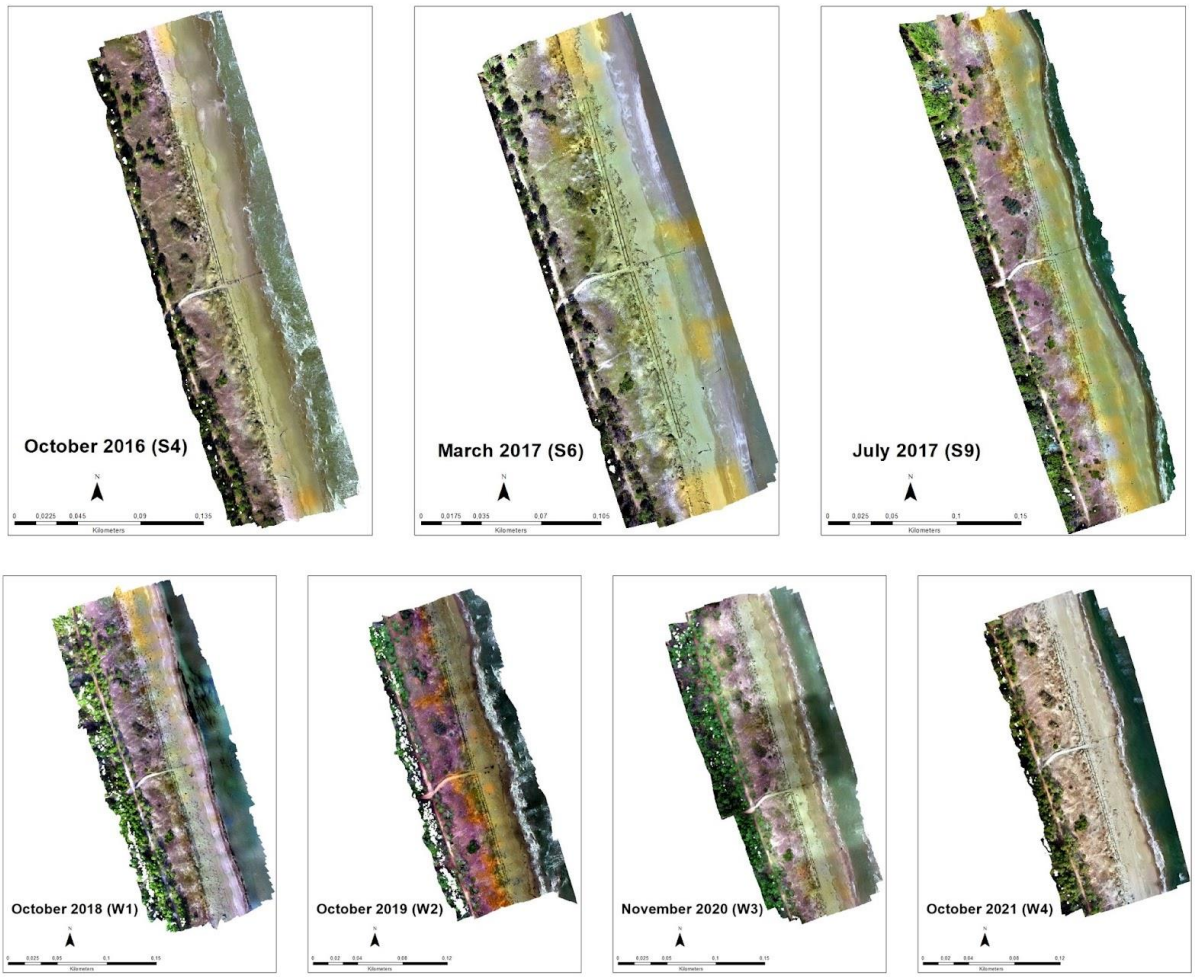

Figure 12. Orthomosaic images of all the topographic surveys.

3.2. DEM validation

Four (4) out of seven (7) surveys – October 2018 (W1), October 2019 (W2), November 2020 (W3) and October 2021 (W4) (Figure 13, Figure 15, Figure 17, Figure 19) have been assessed for elevation model validation since these are the only ones that have ground-truth GPS profiles. Each transect was regressed according to the DEM and GPS elevation values to come up with statistical calculations such as the R^2, RMSE, MAE, and error bias (Table 3).

The October 2018 (W1) survey has 2 GPS profiles, with both R^2 values at 0.97. RMSE values are 0.28 m and 0.17 m while the Mean Absolute Error (MAE) are 0.22 m, 0.11 m and error bias values of 0.2 m and 0.04 m (Figure 14).

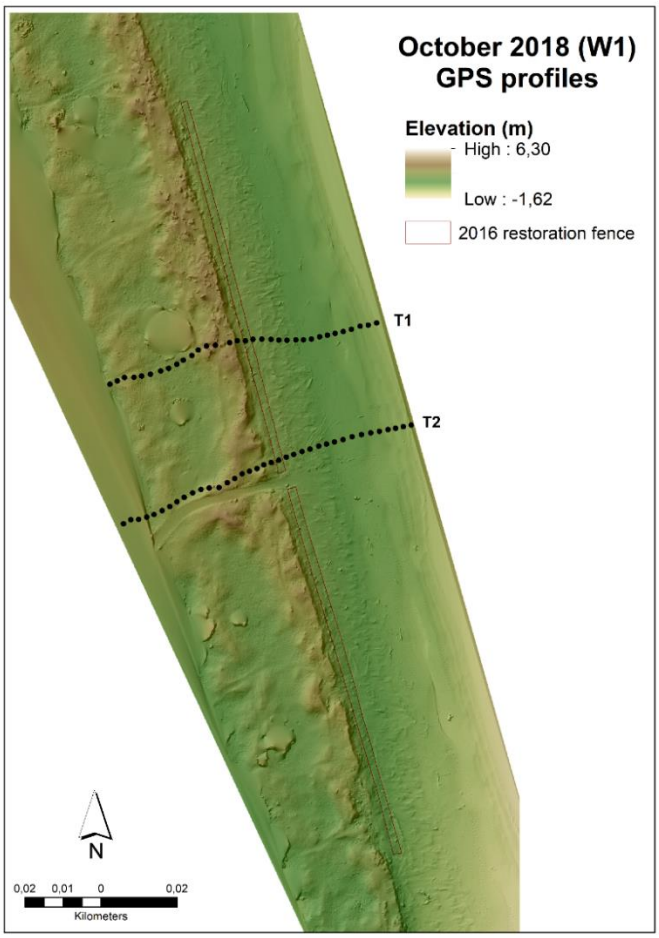

Figure 13. Location of profile transects for October 2018 survey (W1).

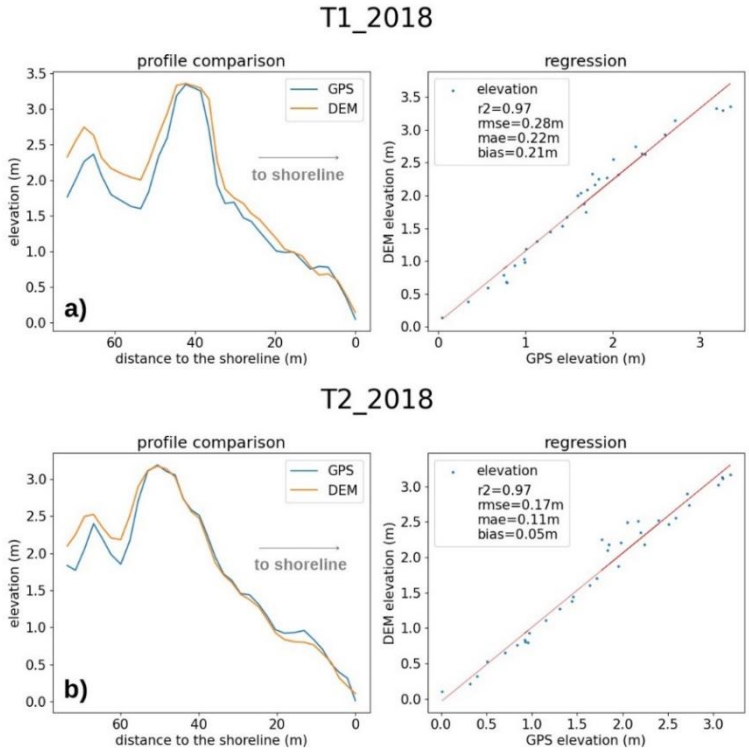

Figure 14. GPS vs DEM profile comparison for 2018 transects.

The October 2019 (W2) survey has a total of four (4) GPS profiles (Figure 15). The correlation between the GPS and DEM profiles all has an R^2 of 0.95 except for Transect 2, which is 0.85. The RMSE values are 0.25 m, 0.19 m, 0.30 m, and 0.20 m. The MAE values are 0.22 m, 0.14 m, 0.23 m, and 0.15 m while the error bias values are 0.21 m, 0.13 m, 0.13 m, and 0.09 m respectively (Figure 16).

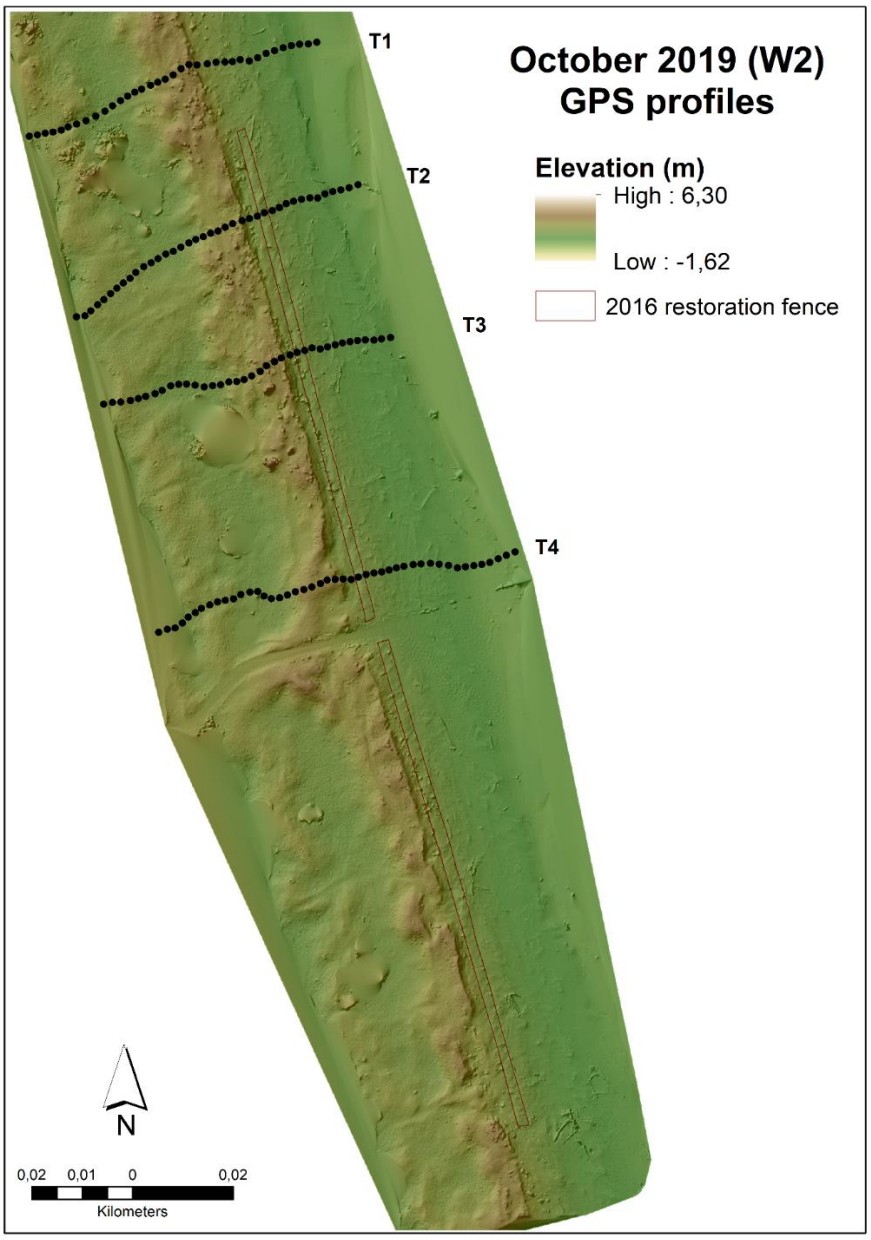

Figure 15. Location of profile transects for October 2019 survey (W2).

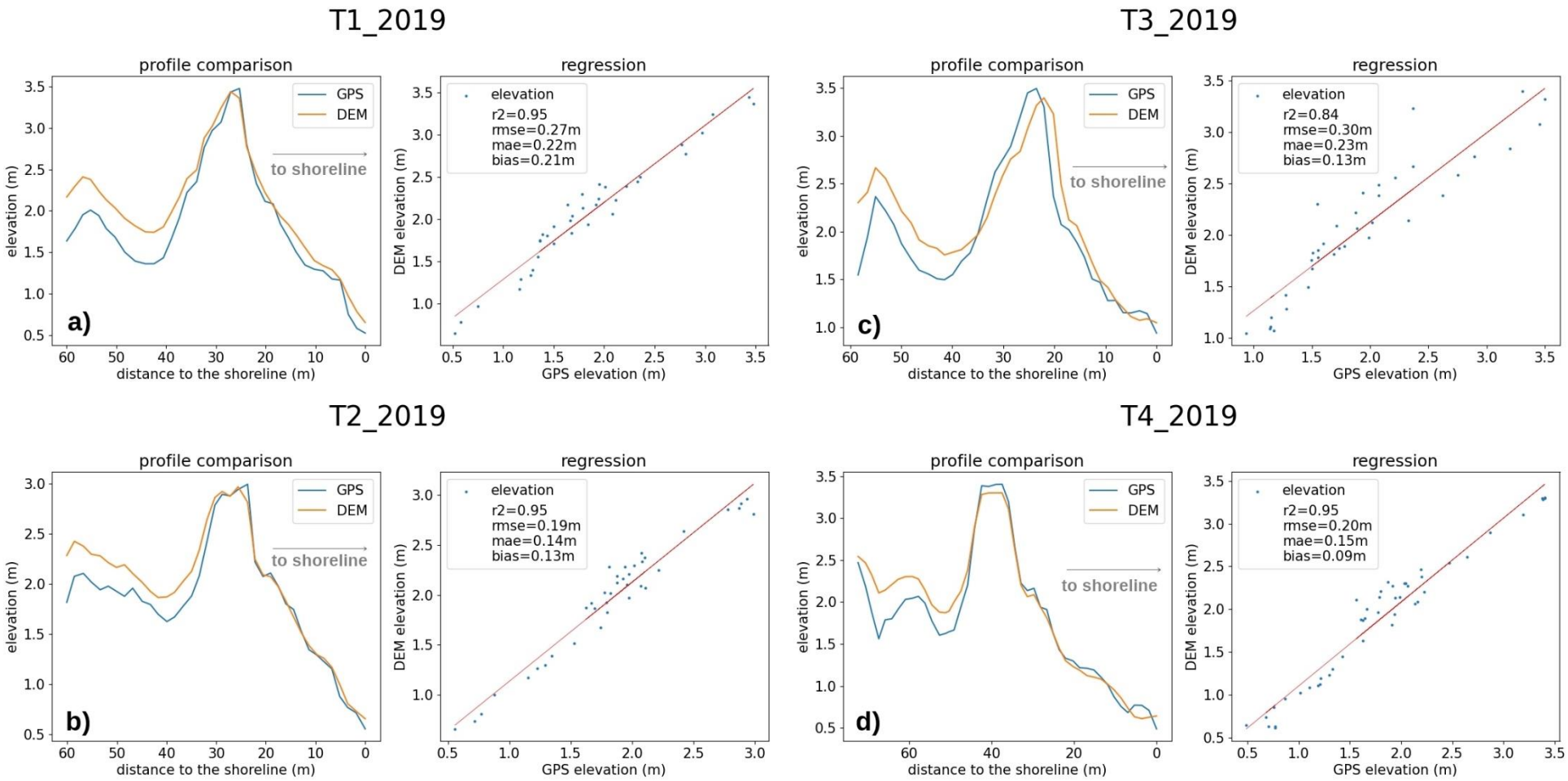

Figure 16. GPS vs DEM profile comparison for 2019 transects.

November 2020 (W3) survey has a total of nine (9) GPS profiles (Figure 17) that were compared to the corresponding DEM values. The R^2 values range from 0.83 to 0.99 while the RMSE values range from 0.15 m to 0.38 m. The MAE and error bias range from 0.12 m to 0.27 m and -0.07 m to 0.20 m, respectively (Figure 18).

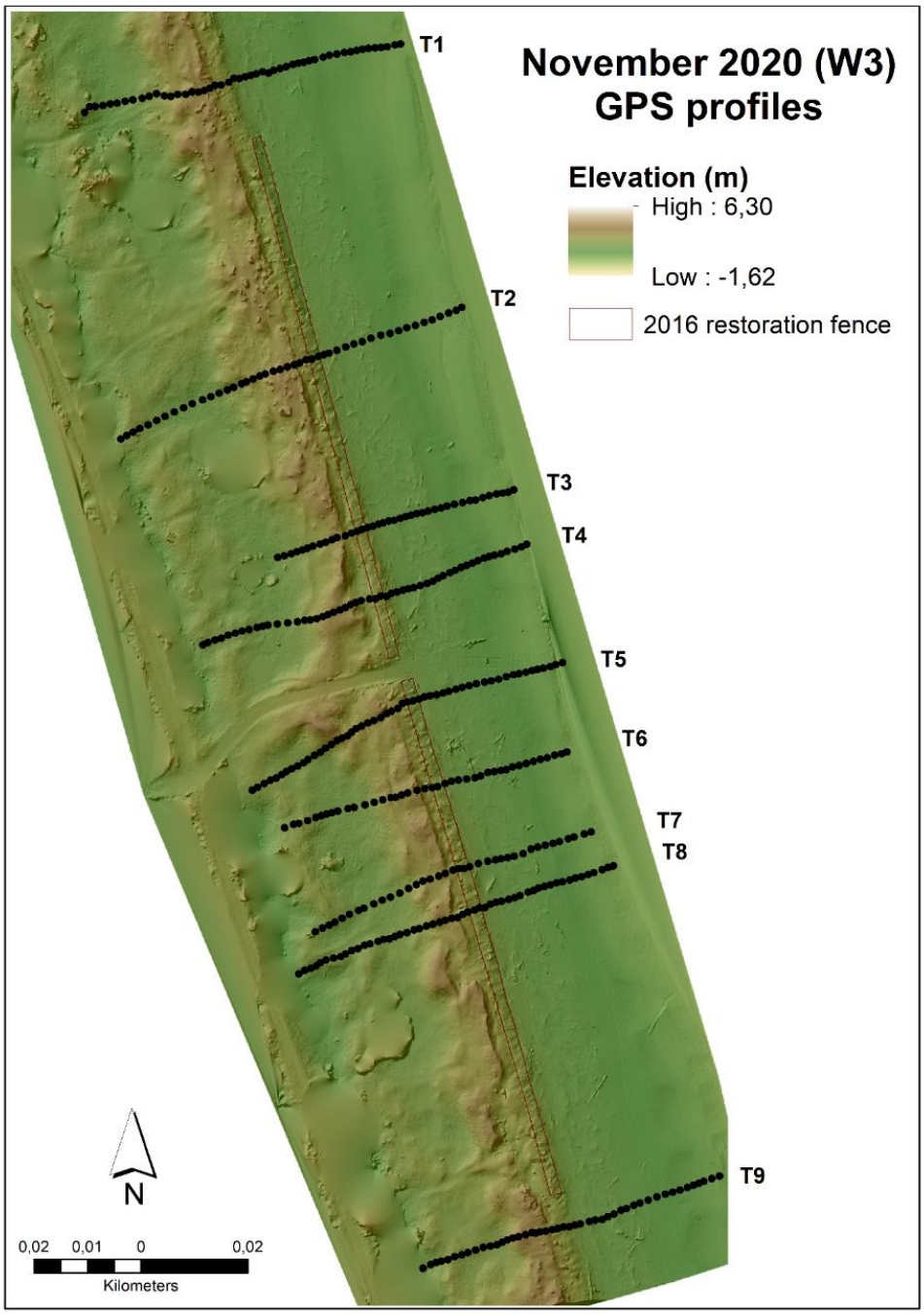

Figure 17. Location of profile transects for November 2020 survey (W3).

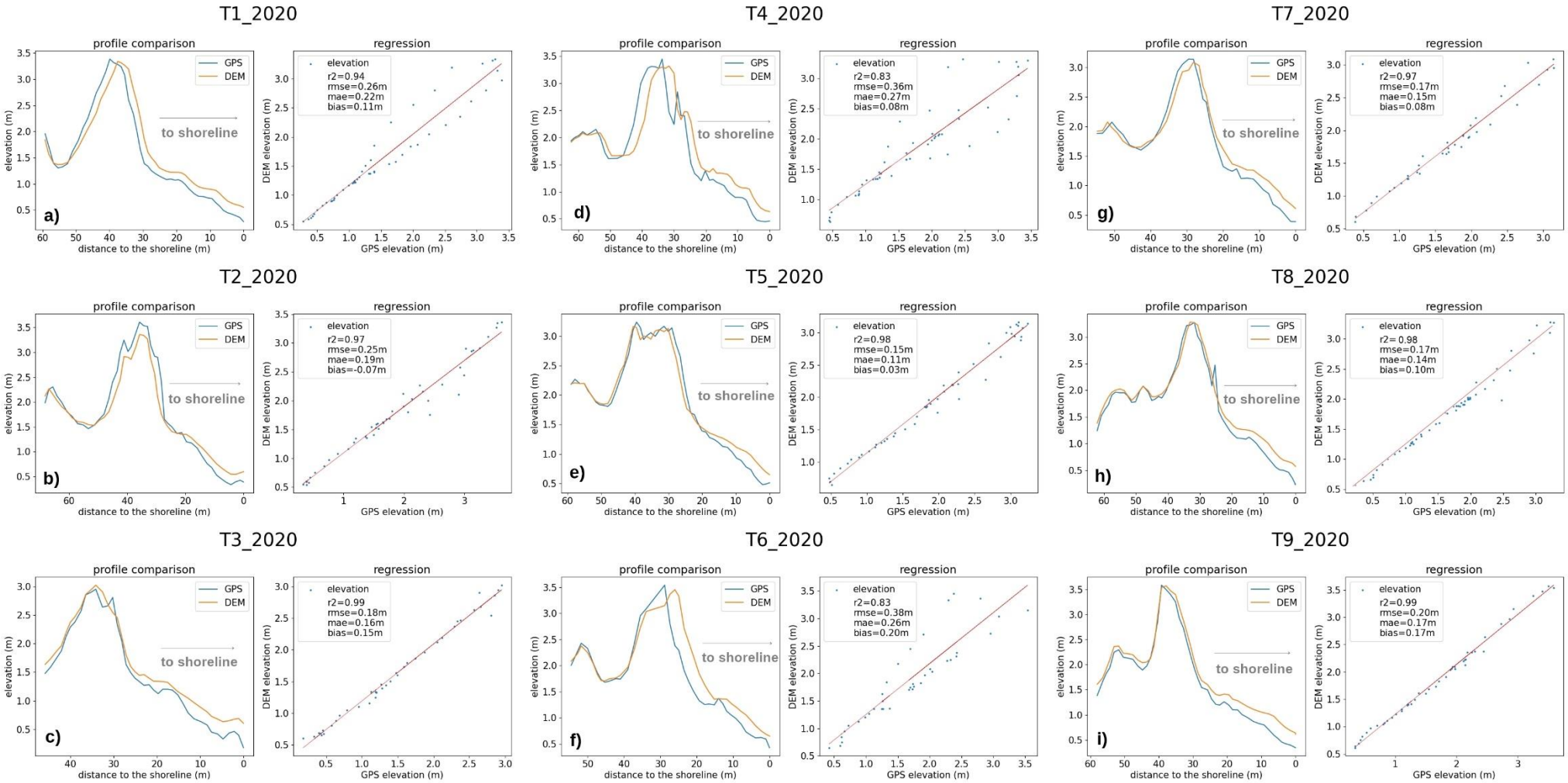

Figure 18. GPS vs DEM profile comparison for 2020 transects.

The last survey, October 2021 (W4) has a total of ten (10) GPS profiles that were compared against the DEM values (Figure 19). The R^2 values range from 0.96 to as high as 1 while the RMSE values range from 0.07 m to 0.16 m. The MAE and error bias values range from 0.07 m to 0.11 m and -0.01 m to 0.05 m, respectively (Figure 20).

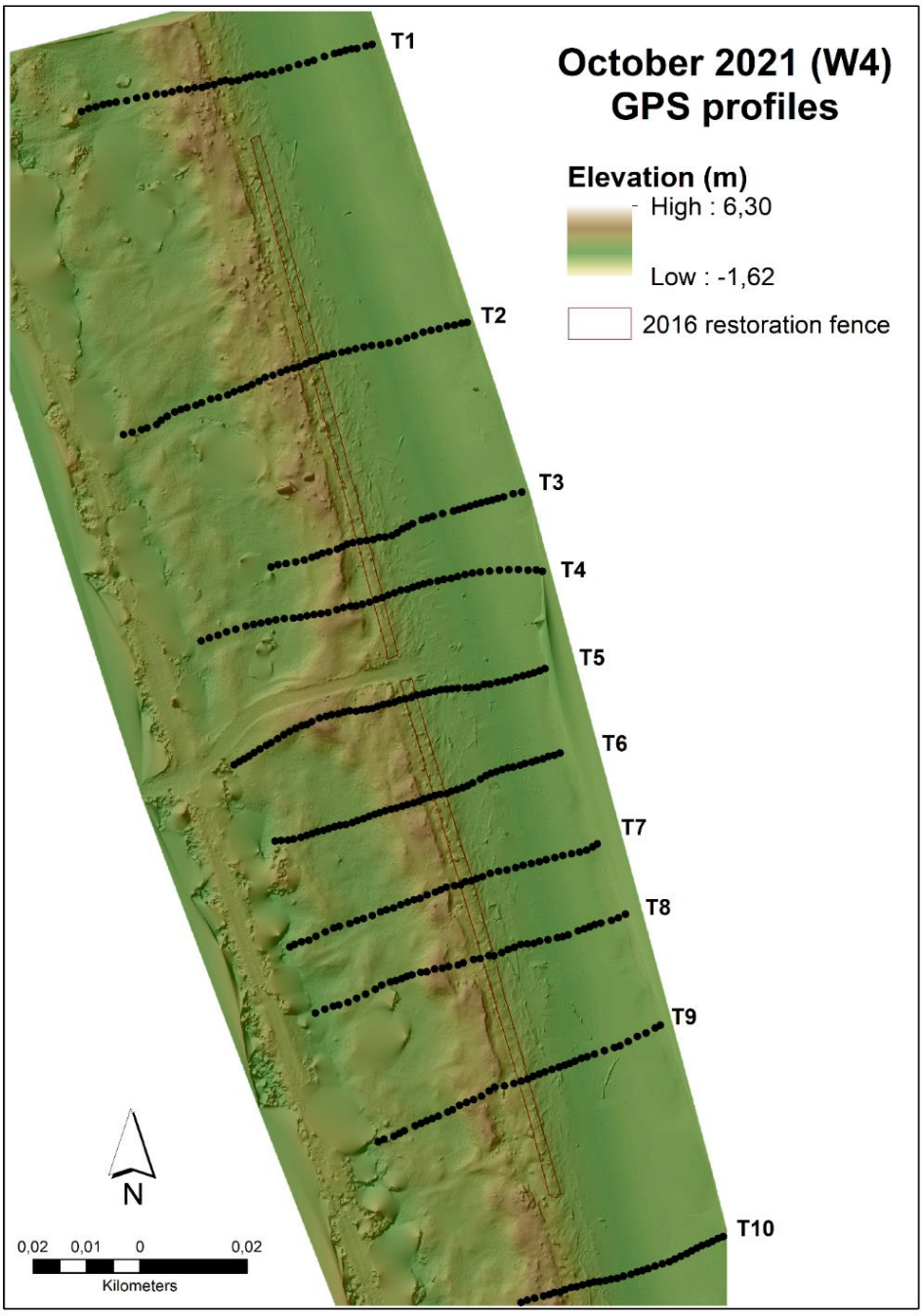

Figure 19. Location of profile transects for October 2021 survey (W4).

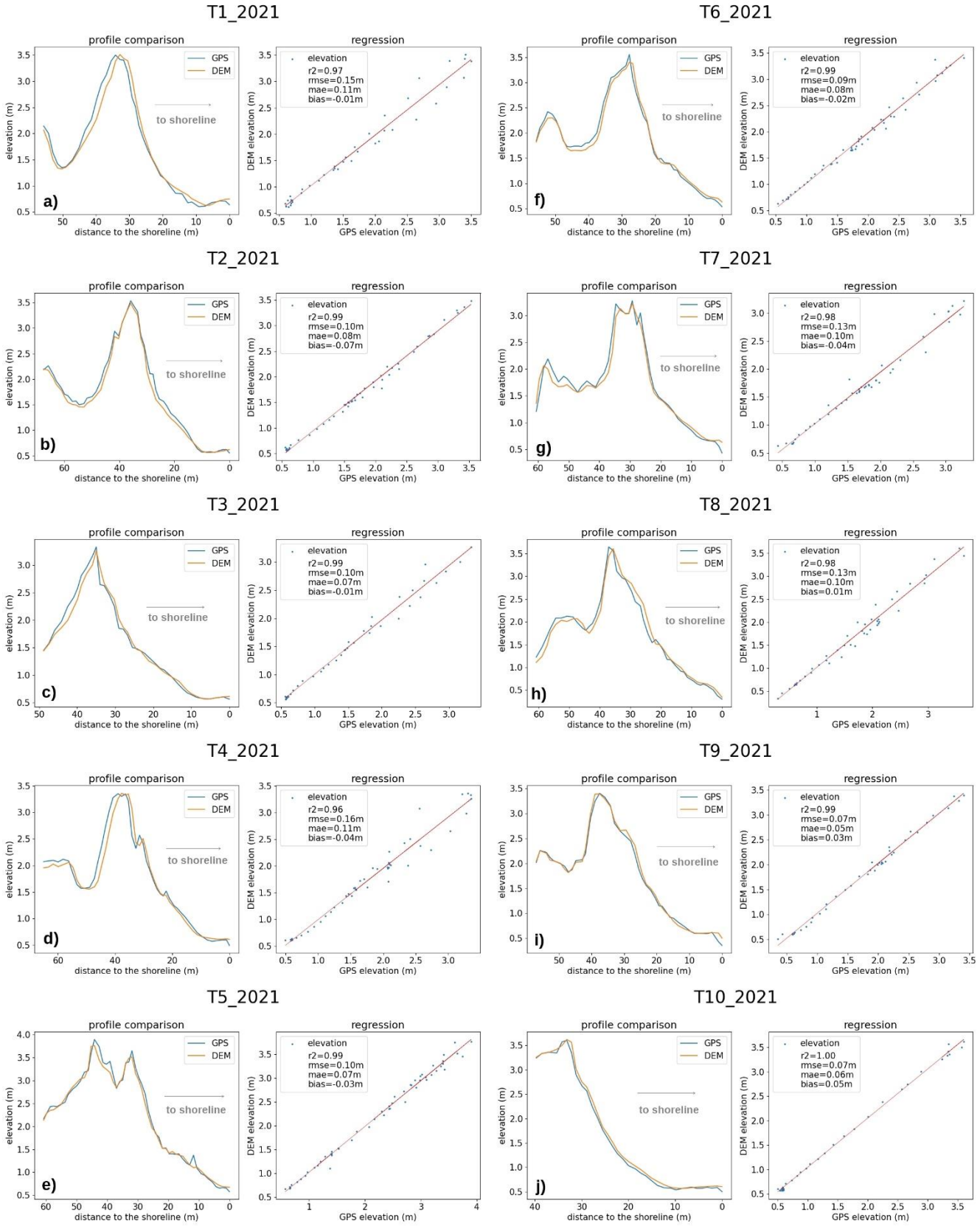

Figure 20. GPS vs DEM profile comparison for 2021 transects.

year	transect	R2	RMSE (m)	MAE (m)	bias (m)
2018	1	0.97	0.28	0.22	0.21
	2	0.97	0.17	0.11	0.05
2019	1	0.95	0.27	0.22	0.21
	2	0.95	0.19	0.14	0.13
	3	0.84	0.30	0.23	0.13
	4	0.95	0.20	0.15	0.09
2020	1	0.94	0.26	0.22	0.11
	2	0.97	0.25	0.19	-0.07
	3	0.99	0.18	0.16	0.15
	4	0.83	0.36	0.27	0.08
	5	0.98	0.15	0.11	0.03
	6	0.83	0.38	0.26	0.20
	7	0.97	0.17	0.15	0.08
	8	0.98	0.17	0.14	0.09
	9	0.99	0.20	0.17	0.17
2021	1	0.97	0.15	0.11	-0.01
	2	0.99	0.10	0.08	-0.07
	3	0.99	0.10	0.07	-0.01
	4	0.96	0.16	0.11	-0.04
	5	0.99	0.10	0.07	-0.03
	6	0.99	0.09	0.08	-0.02
	7	0.98	0.13	0.10	-0.04
	8	0.98	0.13	0.10	0.01
	9	0.99	0.07	0.05	0.03
	10	1.00	0.07	0.06	0.05

Table 3. Summary statistics for all the transects.

3.3. Geomorphic Change Detection (GCD)

The change detection result from the comparison between the October 2021 (W4) and October 2016 (S4) is shown in Figure 21. The goal is to determine the overall sediment change since the establishment of the dune fence in early 2016. Profile comparisons between these elevation models were also performed to see slope changes over time and have an in-depth assessment of the sediment erosion and deposition over time (Figure 23).

Annual geomorphic change detection was also performed to calculate areal change, volumetric change, and vertical change (Figure 22 a, b, c). Aside from the sediment behavior, the annual analysis is done in order to assess the quality of the produced DEMs and understand the possible erroneous values in the GCD result (Table 5, Table 6, Table 7, Table 8).

The summary result of the GCD analysis for October 2021 (W4) versus October 2016 (S4) is shown in Table 4. From the raw data of 9,154 m^2, only 6,020 m^2 of the total area has detectable change after applying the 95% C.I. threshold. In terms of areal change, 2,221 m^2 of the total area had surface lowering while 3,799 m^2 of the total area

had surface raising. Overall, there is a 66% of the area of interest with detectable change.

In terms of volumetric change, a total of 584 m^3 surface lowering and 1,109 m^3 surface raising was calculated out of the thresholded values. A total of 1,692 m^3 of difference has been calculated with a net volume difference of 525 m^3.

For vertical averages, an average depth of 0.26 m and 0.29 m of surface lowering and raising was calculated. The average total thickness of difference is 0.18 m, with a net thickness difference of 0.06 m. In terms of percentage by volume, there is an identified 34% percent elevation lowering and 66% surface raising. The calculated percent imbalance or the departure from the equilibrium is at 16%. The net total volume ratio is at 31%. The detailed description of the metrics is also shown in the Table 4.

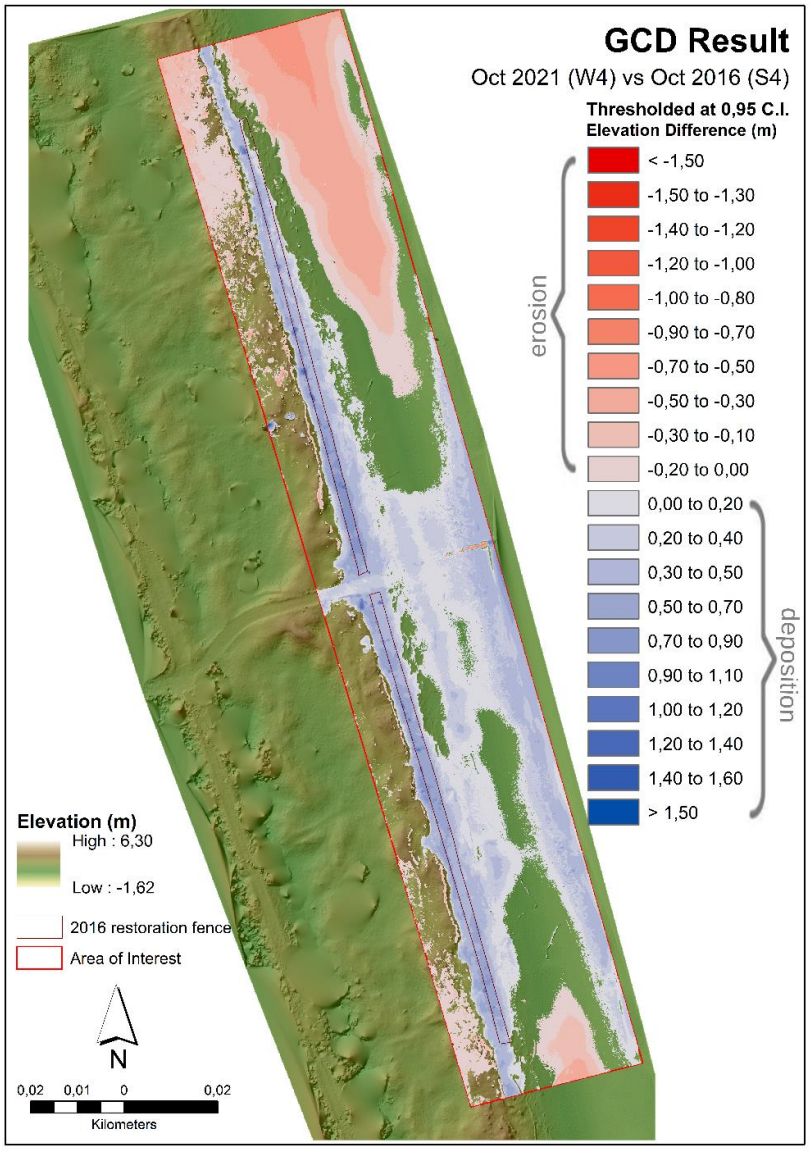

Figure 21. Change Detection result of October 2021 (W4) vs October 2016 (S4) DEM.

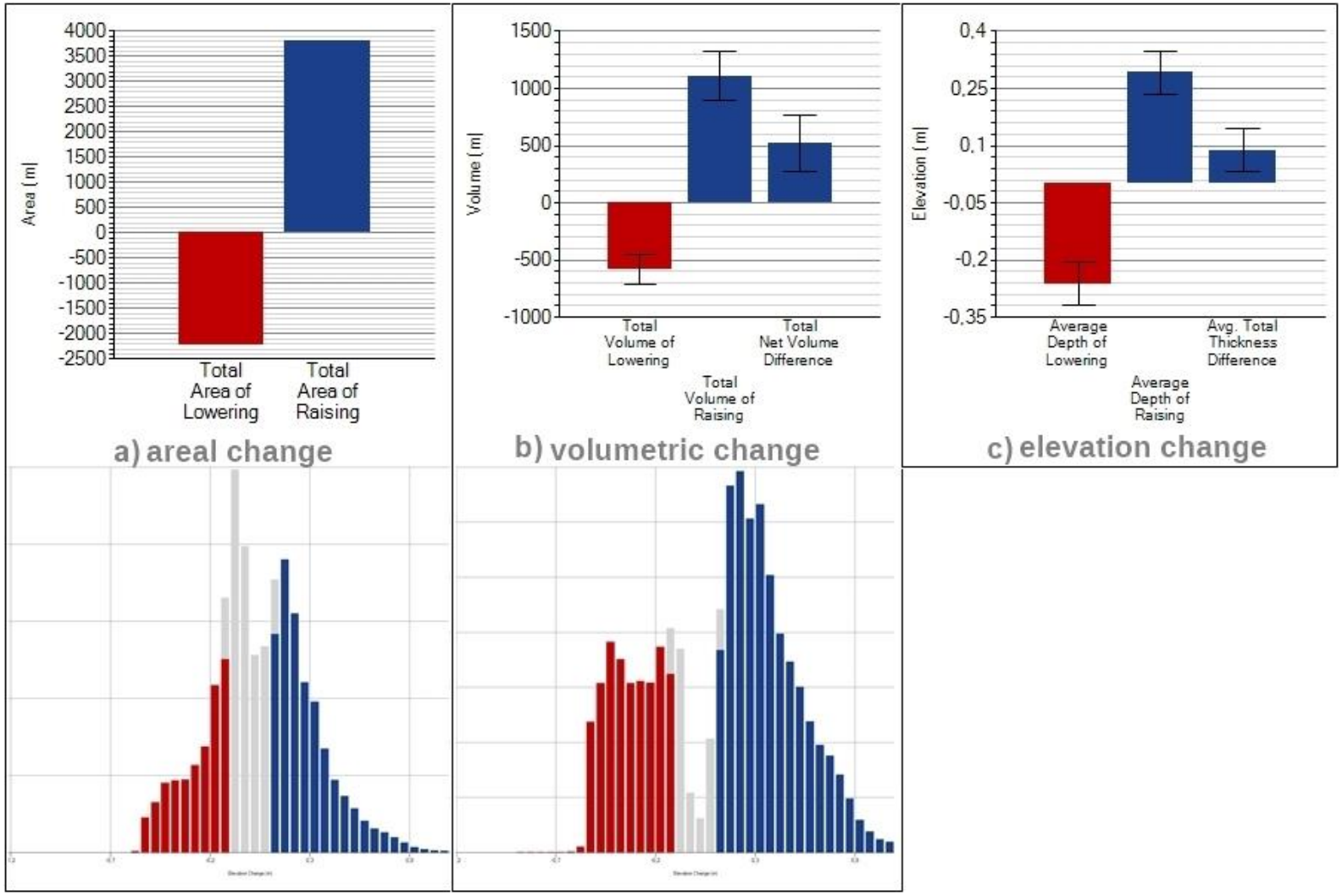

Figure 22. Areal change (a), volumetric change (b), and elevation change (c) of the October 2021 (W4) vs October 2016 (S4) DEM differencing.

Attribute	Raw	Thresholded DoD Estimate:	± Error Volume	% Error	Description
AREAL:					**AREAL METRICS**
Total Area of Surface Lowering (m^2)	4,168	2,221			The amount of area experiencing a lowering of surface elevations
Total Area of Surface Raising (m^2)	4,986	3,799			The amount of area experiencing an increase of surface elevations
Total Area of Detectable Change (m^2)	NA	6,020			The sum of areas experiencing detectable surface elevation changes
Total Area of Interest (m^2)	9,154	NA			The total amount of area under analysis (including detectable and undetectable)
Percent of Area of Interest with Detectable Change	NA	66%			The percent of the total area of interest with detectable changes (i.e. either exceeding the minimum level of detection or with a proability greater then the confidence interval chosen by user)
VOLUMETRIC:			± Error Volume	% Error	**VOLUMETRIC METRICS**
Total Volume of Surface Lowering (m^3)	696	584 ±	124	21.32%	On a cell-by-cell basis, the DoD surface lowering depth (e.g. erosion, cut or deflation) multiplied by cell area and summed
Total Volume of Surface Raising (m^3)	1,177	1,109 ±	213	19.20%	On a cell-by-cell basis, the DoD surface raising (e.g. deposition, fill or inflation) depth multiplied by cell area and summed
Total Volume of Difference (m^3)	1,873	1,692 ±	337	19.93%	The sum of lowering and raising volumes (a measure of total turnover)
Total Net Volume Difference (m^3)	481	525 ±	247	46.99%	The net difference of erosion and depostion volumes (i.e. deposition minus erosion)
VERTICAL AVERAGES:			± Error Thickness	% Error	**VOLUMETRIC METRICS NORMALIZED BY AREA**
Average Depth of Surface Lowering (m)	0.17	0.26 ±	0.06	21.32%	The average depth of lowering (surface lowering volume divided by surface lowering area)
Average Depth of Surface Raising (m)	0.24	0.29 ±	0.06	19.20%	The average depth of raising (surace raising volume divided by surface raising area)
Average Total Thickness of Difference (m) for Area of Interest	0.20	0.18 ±	0.04	19.93%	The total volume of difference divided by the area of interest (a measure of total turnover thickness in the analysis area)
Average Net Thickness Difference (m) for Area of Interest	0.05	0.06 ±	0.03	46.99%	The total net volume of difference divided by the area of interest (a measure of resulting net change within the analysis area)
Average Total Thickness of Difference (m) for Area With Detectable Change	NA	0.28 ±	0.06	19.93%	The total volume of difference divided by the total area of detectable change (a measure of total turnover thickness where there was detectable change)
Average Net Thickness Difference (m) for Area with Detectable Change	NA	0.09 ±	0.04	46.99%	The total net volume of difference dividied by the total area of detectable change (a measure of resulting net change where the was detectable change)
PERCENTAGES (BY VOLUME)					**NORMALIZED PERCENTAGES**
Percent Elevation Lowering	37%	34%			Percent of Total Volume of Difference that is surface lowering
Percent Surface Raising	63%	66%			Percent of Total Volume of Difference that is surface raising
Percent Imbalance (departure from equilibrium)	13%	16%			The percent depature from a 50%-50% equilibirum lowering/raising (i.e. erosion/deposition) balance (a normalized indication of the magnitude of the net difference)
Net to Total Volume Ratio	26%	31%			The ratio of net volumetric change divided by total volume of change (a measure of how much the net trend explains of the total turnover)

Table 4. Tabular summary of the change detection calculation of October 2021 (W4) vs October 2016 (S4) DEM.

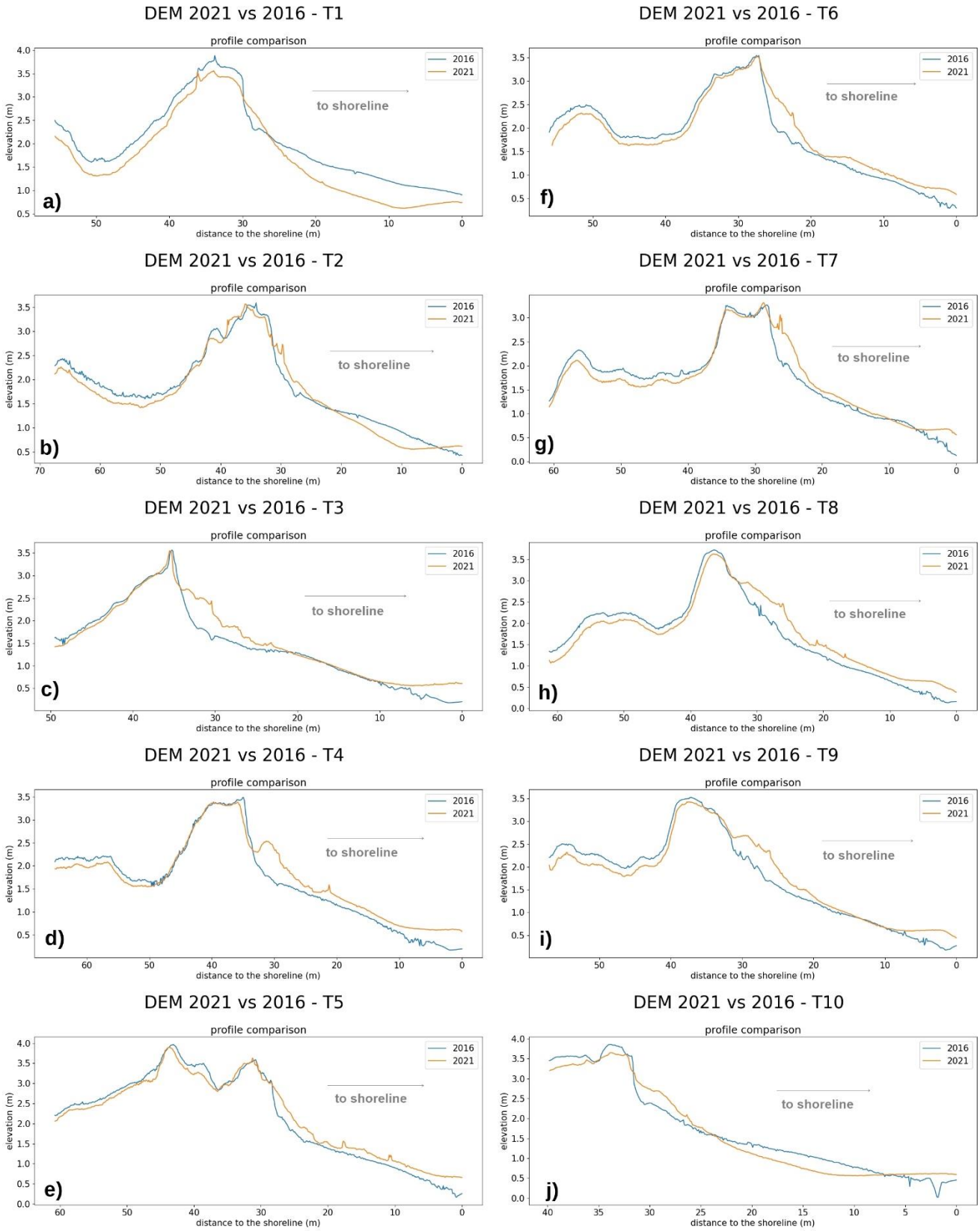

Figure 23. Transect profiles comparison of October 2021 and October 2016 DEM.

Figure 31 and Figure 32 in the Appendix and Table 5, Table 6, Table 7, and Table 8 show the annual comparison between surveys.

AREAL **min Probabilistic at 0,95 Confidence Level within dunes**

	Total Area of Surface Lowering (m^2)		Total Area of Surface Raising (m^2)		Total Area of Detectable Change (m^2)	Total Area of Interest (m^2)	AOI % with Detectable Change
	Raw	Thresholded DoD Estimate	Raw	Thresholded DoD Estimate	Thresholded DoD Estimate		
Mar 2017 (S6) vs Oct 2016 (S4)	*2871.72*	781.86	*5692.74*	2882.83	3664.69	8564.46	43%
Jul 2017 (S9) vs Mar 2017 (S6)	*5644.14*	3552.33	*2922.06*	659.72	4212.05	8566.2	49%
Oct 2018 (W1) vs Jul 2017 (S9)	*4947.33*	3462.93	*4207.26*	2660.66	6123.59	9154.59	67%
Oct 2019 (W2) vs Oct 2018 (W1)	*3016.45*	1405.1	*6020.06*	4621.55	6026.65	9036.51	67%
Nov 2020 (W3) vs Oct 2019 (W2)	*2655.25*	529.43	*6380.09*	2014.18	2543.61	9035.34	28%
Oct 2021 (W4) vs Nov 2020 (W3)	*5146.68*	2382.75	*4005.27*	303.63	2686.38	9151.95	29%

Table 5. Summary table of the annual areal change.

VOLUMETRIC

	Total Volume of Surface Lowering (m^3)				Total Volume of Surface Raising (m^3)			
	Raw	Thresholded DoD Estimate	Error	% Error	Raw	Thresholded DoD Estimate	Error	% Error
Mar 2017 (S6) vs Oct 2016 (S4)	*201.26*	120.52	± 38	32%	*830.32*	708.86	± 140	20%
Jul 2017 (S9) vs Mar 2017 (S6)	*1845.74*	1698.84	± 311	18%	*332.00*	167.04	± 58	35%
Oct 2018 (W1) vs Jul 2017 (S9)	*2268.76*	2115.14	± 328	16%	*1253.79*	1088.12	± 252	23%
Oct 2019 (W2) vs Oct 2018 (W1)	*360.21*	267.24	± 78	29%	*2778.83*	2707.71	± 258	10%
Nov 2020 (W3) vs Oct 2019 (W2)	*296.70*	165.61	± 48	29%	*906.50*	523.56	± 183	35%
Oct 2021 (W4) vs Nov 2020 (W3)	*912.39*	705.04	± 210	30%	*285.29*	73.87	± 27	36%

	Total Volume of Difference (m^3)				Total Net Volume Difference (m^3)			
	Raw	Thresholded	Error	% Error	Raw	Thresholded	Error	%Error
Mar 2017 (S6) vs Oct 2016 (S4)	*1031.58*	829.39	± 178	22%	*629.05*	588.34	± 145	25%
Jul 2017 (S9) vs Mar 2017 (S6)	*2177.74*	1865.88	± 368	20%	*2718.00*	1866.00	± 368	20%
Oct 2018 (W1) vs Jul 2017 (S9)	*3522.54*	3203.26	± 581	18%	*-1014.97*	-1027.01	± 414	-40%
Oct 2019 (W2) vs Oct 2018 (W1)	*3139.04*	2974.94	± 337	11%	*2418.62*	2440.47	± 270	11%
Nov 2020 (W3) vs Oct 2019 (W2)	*1203.20*	689.18	± 231	43%	*609.79*	357.95	± 189	53%
Oct 2021 (W4) vs Nov 2020 (W3)	*1197.68*	778.91	± 236	30%	*-627.10*	-631.17	± 211	-33%

Table 6. Summary table of the annual volumetric change.

VERTICAL AVERAGES

	Average Depth of Surface Lowering (m)				Average Depth of Surface Raising (m)			
	Raw	Thresholded	Error	% Error	Raw	Thresholded	Error	%Error
Mar 2017 (S6) vs Oct 2016 (S4)	*0.07*	0.15	± 0.05	32%	*0.15*	0.25	± 0.05	32%
Jul 2017 (S9) vs Mar 2017 (S6)	*0.33*	0.48	± 0.09	18%	*0.11*	0.25	± 0.09	35%
Oct 2018 (W1) vs Jul 2017 (S9)	*0.46*	0.61	± 0.09	16%	*0.30*	0.41	± 0.09	23%
Oct 2019 (W2) vs Oct 2018 (W1)	*0.12*	0.19	± 0.06	29%	*0.46*	0.59	± 0.06	10%
Nov 2020 (W3) vs Oct 2019 (W2)	*0.11*	0.31	± 0.09	29%	*0.14*	0.26	± 0.09	35%
Oct 2021 (W4) vs Nov 2020 (W3)	*0.18*	0.30	± 0.09	30%	*0.07*	0.24	± 0.09	36%

	AOI Average Total Thickness of Difference (m)				AOI Average Net Thickness Difference (m)			
	Raw	Thresholded	Error	% Error	Raw	Thresholded	Error	%Error
Mar 2017 (S6) vs Oct 2016 (S4)	*0.12*	0.10	± 0.02	22%	*0.07*	0.07	± 0.02	25%
Jul 2017 (S9) vs Mar 2017 (S6)	*0.25*	0.22	± 0.04	20%	*-0.18*	-0.18	± 0.04	-21%
Oct 2018 (W1) vs Jul 2017 (S9)	*0.38*	0.35	± 0.06	18%	*-0.11*	-0.11	± 0.05	-40%
Oct 2019 (W2) vs Oct 2018 (W1)	*0.35*	0.33	± 0.04	11%	*0.27*	0.27	± 0.03	11%
Nov 2020 (W3) vs Oct 2019 (W2)	*0.13*	0.08	± 0.03	34%	*0.07*	0.04	± 0.02	53%
Oct 2021 (W4) vs Nov 2020 (W3)	*0.13*	0.09	± 0.03	30%	*-0.07*	-0.07	± 0.02	-33%

	ADC Avg Total Thickness of Difference (m)			ADC Average Net Thickness of Difference (m)		
	Thresholded	Error	%Error	Thresholded	Error	%Error
Mar 2017 (S6) vs Oct 2016 (S4)	0.23	± 0.05	22%	0.16	± 0.04	25%
Jul 2017 (S9) vs Mar 2017 (S6)	0.44	± 0.09	20%	-0.36	± 0.08	-21%
Oct 2018 (W1) vs Jul 2017 (S9)	0.52	± 0.09	18%	-0.17	± 0.07	-40%
Oct 2019 (W2) vs Oct 2018 (W1)	0.49	± 0.06	11%	0.40	± 0.04	11%
Nov 2020 (W3) vs Oct 2019 (W2)	0.27	± 0.09	34%	0.14	± 0.07	53%
Oct 2021 (W4) vs Nov 2020 (W3)	0.29	± 0.09	30%	-0.23	± 0.08	-33%

Table 7. Summary table of the annual change by vertical averages.

PERCENTAGES BY VOLUME

	Percent Elevation Lowering Thresholded	Percent Elevation Raising Thresholded	Percent Imbalance (departure from equilibrium) Thresholded	Net to Total Volume Ratio Thresholded
Mar 2017 (S6) vs Oct 2016 (S4)	15%	85%	35%	71%
Jul 2017 (S9) vs Mar 2017 (S6)	91%	9%	-35%	-41%
Oct 2018 (W1) vs Jul 2017 (S9)	66%	34%	-16%	-32%
Oct 2019 (W2) vs Oct 2018 (W1)	9%	91%	41%	82%
Nov 2020 (W3) vs Oct 2019 (W2)	24%	76%	26%	52%
Oct 2021 (W4) vs Nov 2020 (W3)	91%	9%	-41%	-81%

Table 8. Summary table of the annual change by percentage by volume.

3.4. Vegetation cover change

2016 and 2021 orthomosaics were used in the vegetation cover change assessment. All seven (7) transects were individually examined at an individual grid level to identify whether each centroid of the grid is either vegetated, bare sand, or with logs and debris (Figure 24).

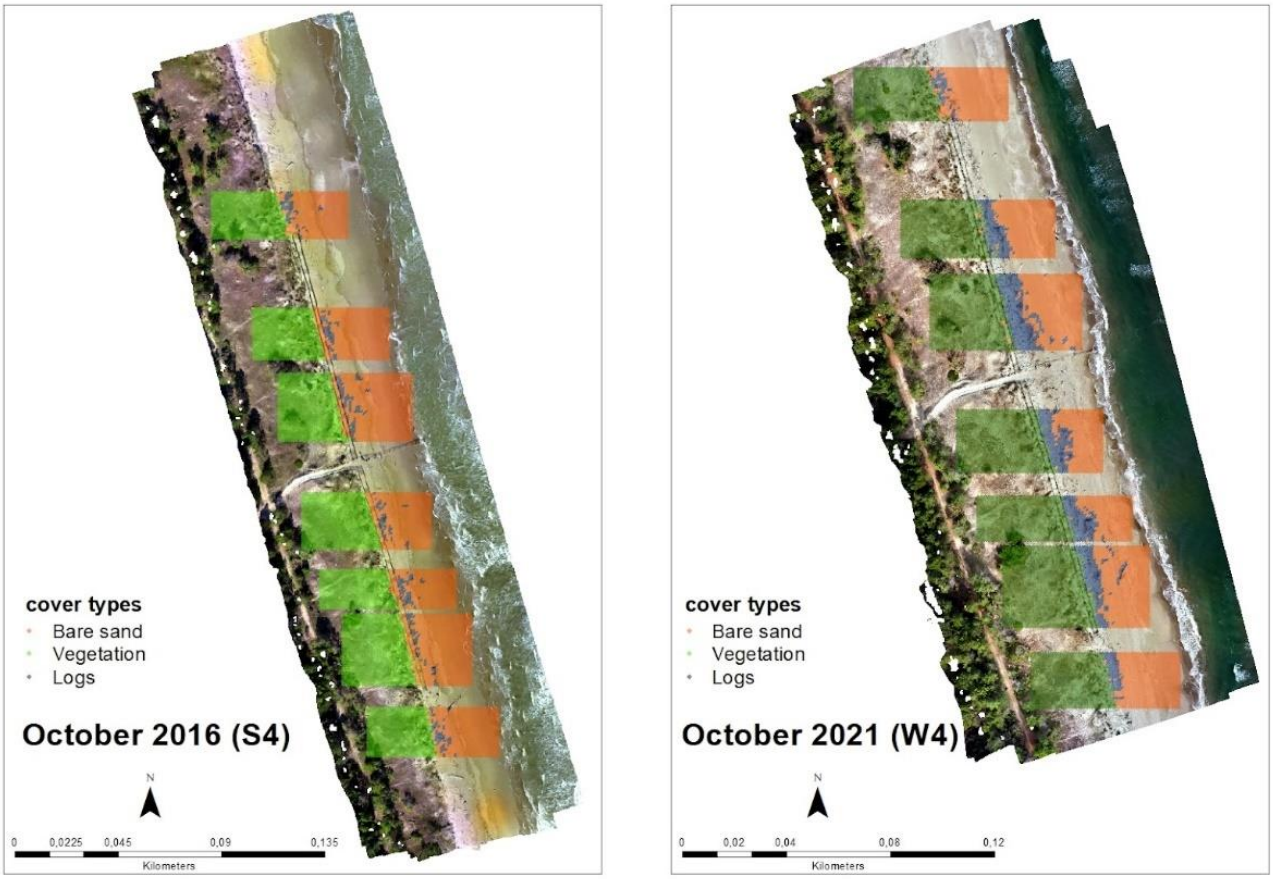

Figure 24. Vegetation cover change between October 2016 (S4) and October 2021 (W4).

The point density of the cover types in each transect were used to come up with a percentage calculation to represent the change (Figure 25 and Table 9). Overall, there was an increase in the cover extent of vegetation and areas with logs or debris. Consequently, an obvious decrease in bare sand extent has been noticeable as well. A sample zoom-in images between the two datasets are shown in Figure 26.

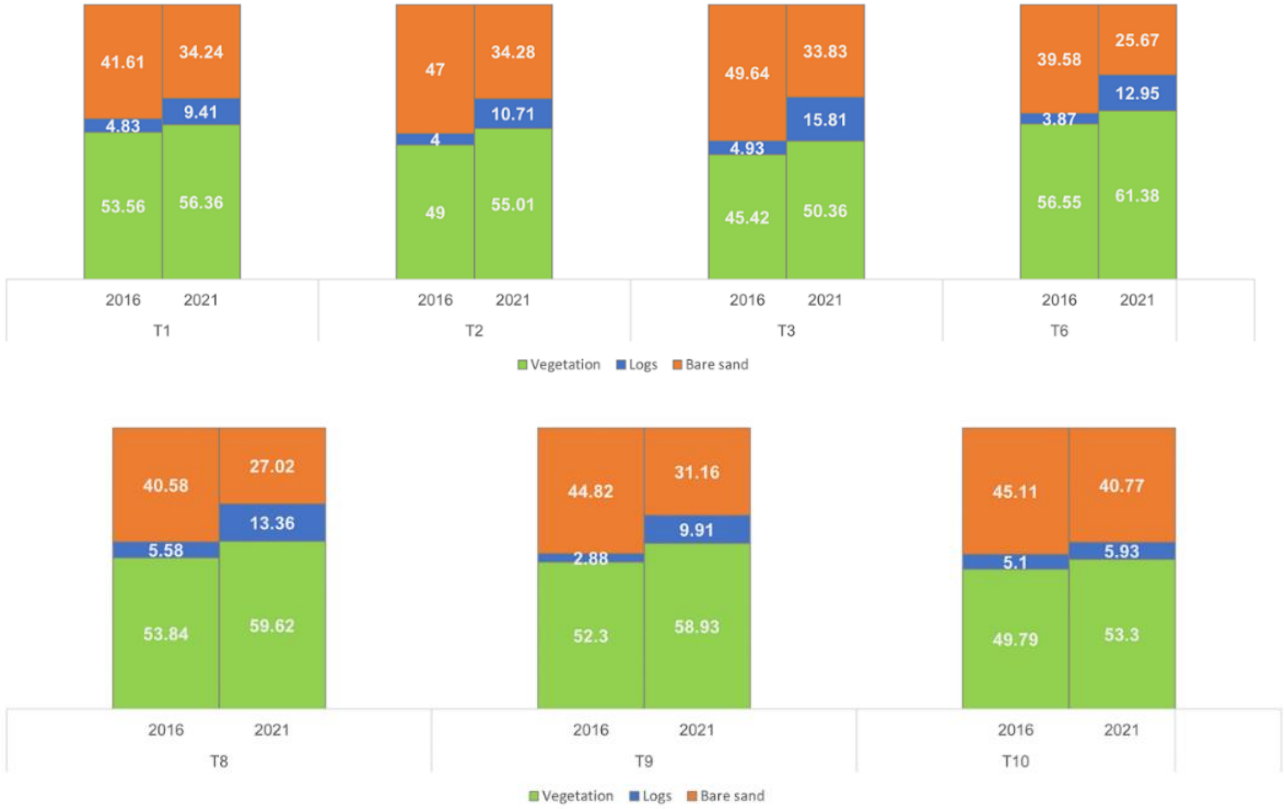

Figure 25. Percentage cover comparison between 2016 and 2021.

Transects	Percentage cover											
	2016			2021			change			% change		
	Vegetation	Logs	Bare sand	Vegetation	Logs	Bare sand	Vegetation	Logs	Bare sand	Vegetation	Logs	Bare sand
T1	53.6	4.8	41.6	56.4	9.4	34.2	2.8	4.6	-7.4	5.2	94.8	-17.7
T2	49.0	4.0	47.0	55.0	10.7	34.3	6.0	6.7	-12.7	12.3	167.8	-27.1
T3	45.4	4.9	49.6	50.4	15.8	33.8	4.9	10.9	-15.8	10.9	220.7	-31.8
T6	56.6	3.9	39.6	61.4	13.0	25.7	4.8	9.1	-13.9	8.5	234.6	-35.1
T8	53.8	5.6	40.6	59.6	13.4	27.0	5.8	7.8	-13.6	10.7	139.4	-33.4
T9	52.3	2.9	44.8	58.9	9.9	31.2	6.6	7.0	-13.7	12.7	244.1	-30.5
T10	49.8	5.1	45.1	53.3	5.9	40.8	3.5	0.8	-4.3	7.0	16.3	-9.6

Table 9. Percent cover change between 2016 and 2021.

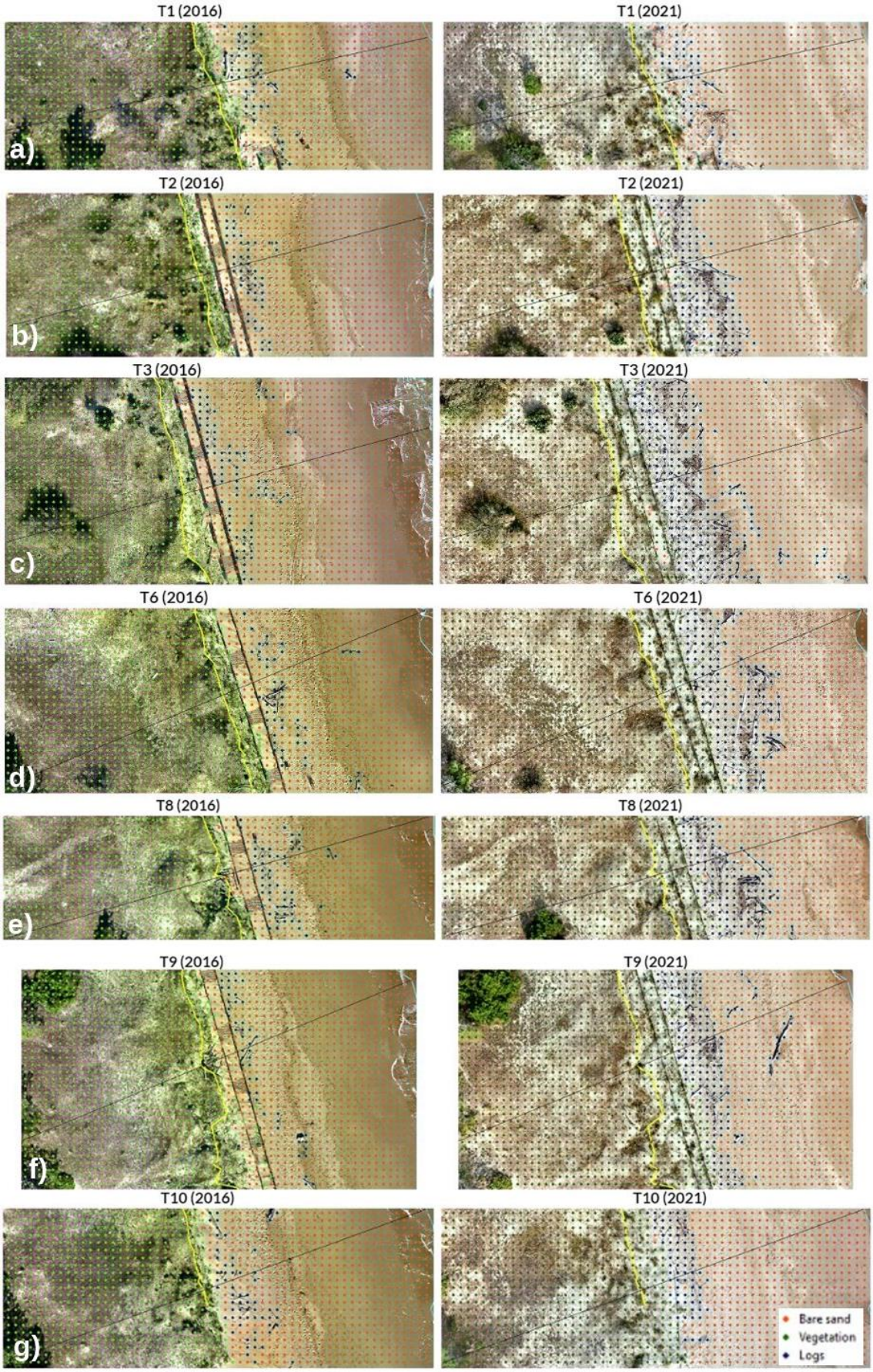

Figure 26. Zoomed-in images of the vegetation cover change along the transects between 2016 and 2021.

3.5. Marine-meteo data

3.5.1. ERA5 reanalysis data

There is no extreme high value in terms of significant wave height (SWH) (Figure 27b) during the period 2016 to 2021. About 0.7 m of wave heights were observed between late autumn to winter (October to February).

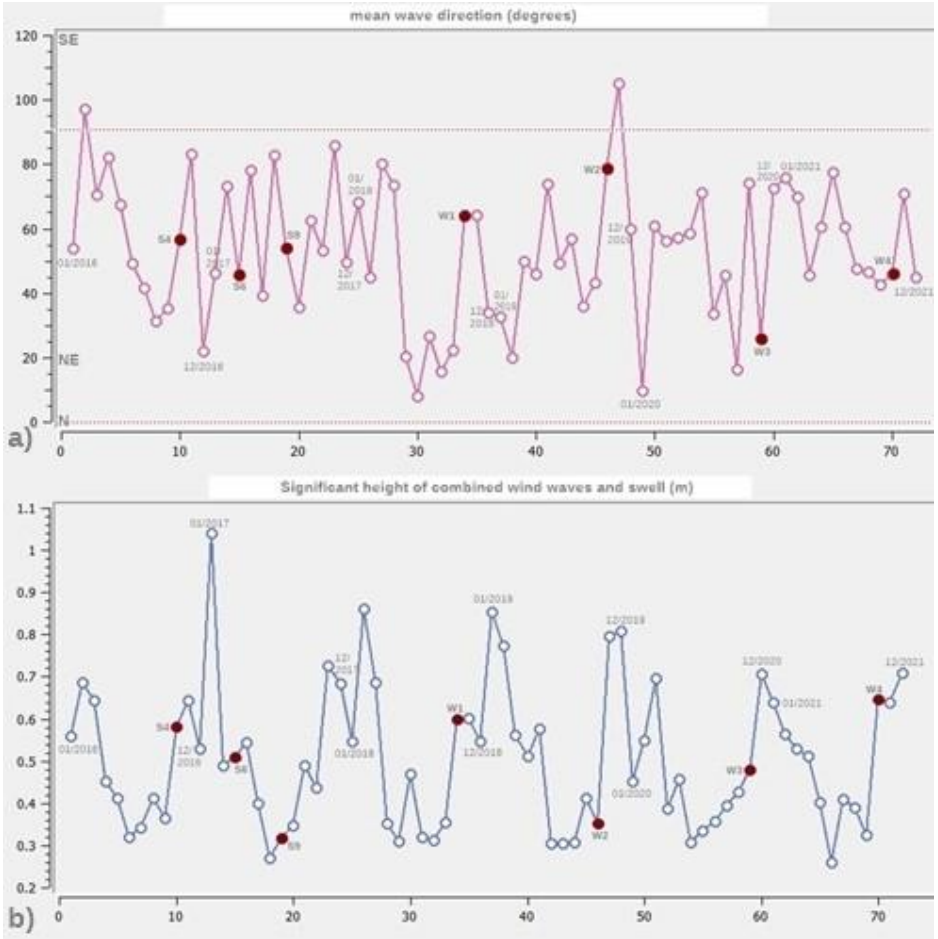

Figure 27. Historical monthly data of the wave parameters from 2016 to 2021. The red points are the month of the survey dates; X-axes are the months, and the Y-axes represents the wave direction in degrees (a) and wave height in meters (b).

For the wind speed, the highest monthly record was in May 2021 with more than 3.2 ms^{-1} (Figure 28a). This parameter is the horizontal speed of the wind at a height of 10 meters above the ground. Both the eastward and the northward parameters are also shown in Figure 28b, c. Wind speeds of above 3 m s^{-1} have been evident also in most of the winter months, which can be attributed to Bora winds.

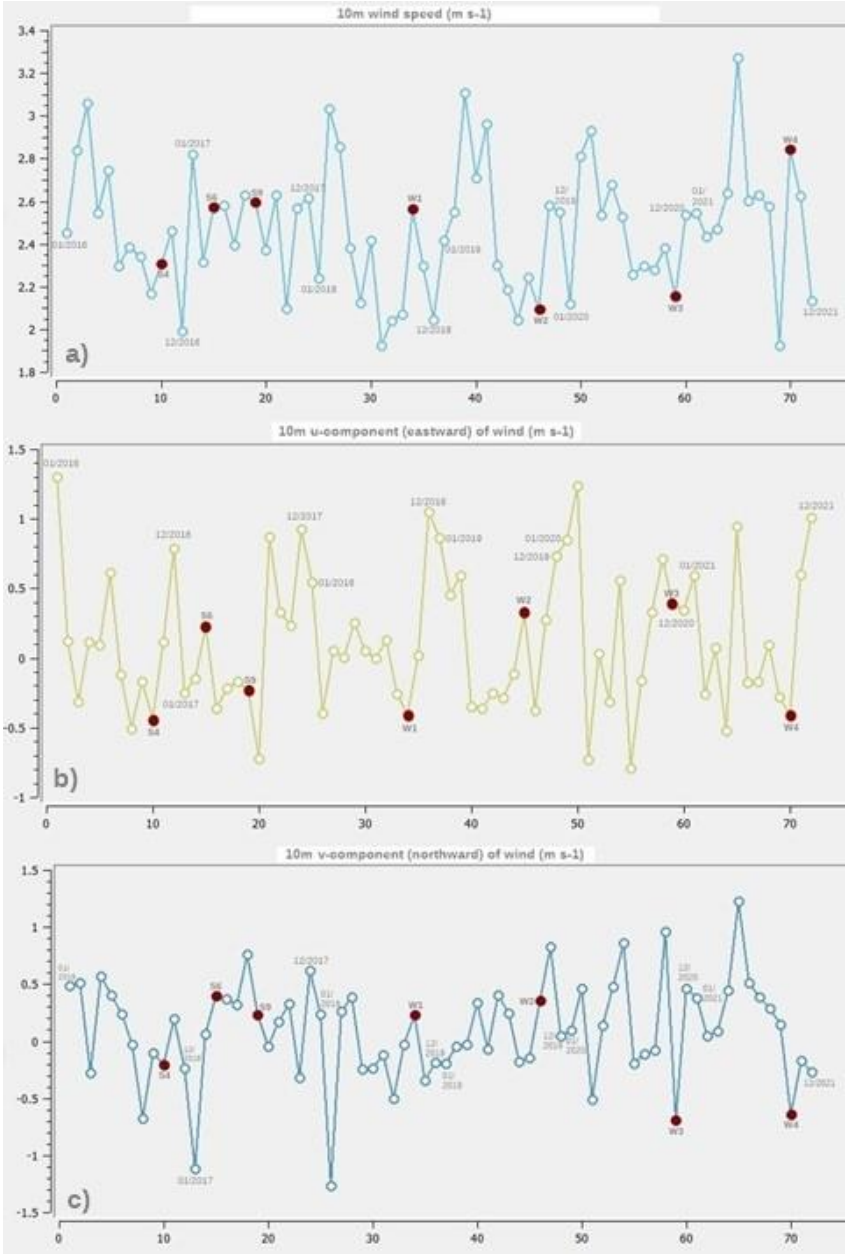

Figure 28. Historical monthly data of the wind parameters from 2016 to 2021. The red points are the month of the survey dates. X- axes are the months, and Y-axes are the wind component units in ms^{-1}.

3.5.2. Arpae 2007-2020 wave buoy data

The wave buoy data in Cesenatico provided annual data for SWH and storm surge information. The majority of the stronger waves (0.2 m to 4 m) are from NE and ENE. Waves blown from the eastern side are more frequent from 2007 to 2020 but are relatively weaker (0.2 m to 2.5 m) as shown in Figure 29.

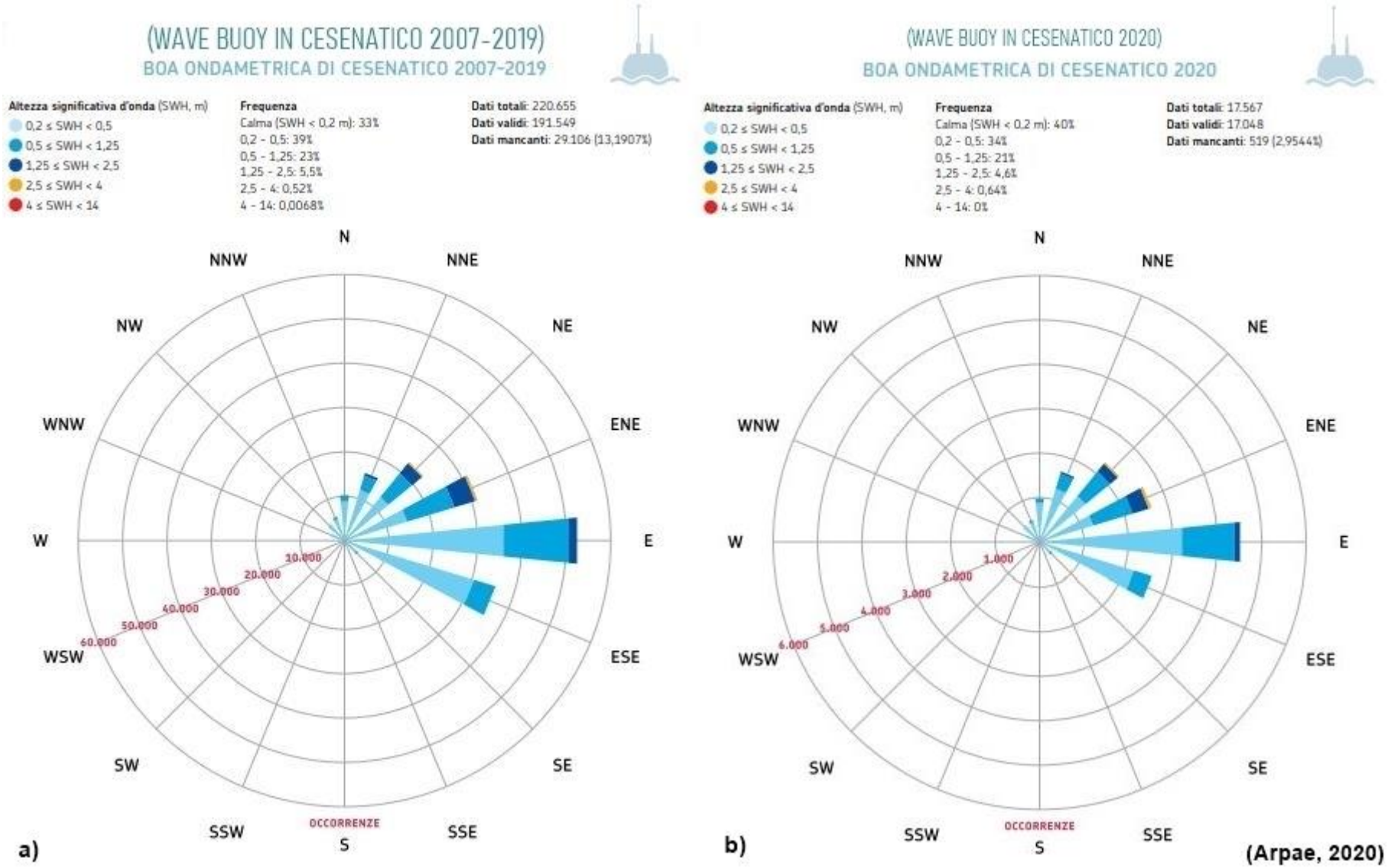

Figure 29. Significant wave height and frequency for 2007-2019 (a) and 2020 (b).

The 2016 to 2020 annual information was extrapolated from the 2007-2020 time-series data (Table 10). The number of storm surges per year ranges from 17 to 24, with an average duration of 12.8 to 27.9 hours. There were no significant or extreme storm surge event within the time frame since the normalized energy was only between 41.8 m^2h to 111.4 m^2h. According to the storm surge class by Arpae (Figure 30), the values only fall within weak and moderate classes.

Year	# of storm surge	Total duration (h)	Ave. Duration (h)	Normalized energy (m^2h)	Ave. SWH (m)	Max SWH (m)	Max SL during storm surge (m)
2016	23	343	14.9	55.1	1.80	3.11	0.93
2017	17	325	19.1	95.9	1.89	3.68	0.87
2018	15	419	27.9	111.4	1.88	3.10	1.06
2019	24	307.5	12.8	41.8	1.67	2.10	1.16
2020	18	340.5	18.9	76.3	1.85	3.11	1.03

Table 10. Wave buoy information from 2016 to 2020 extracted from Arpae, 2020.

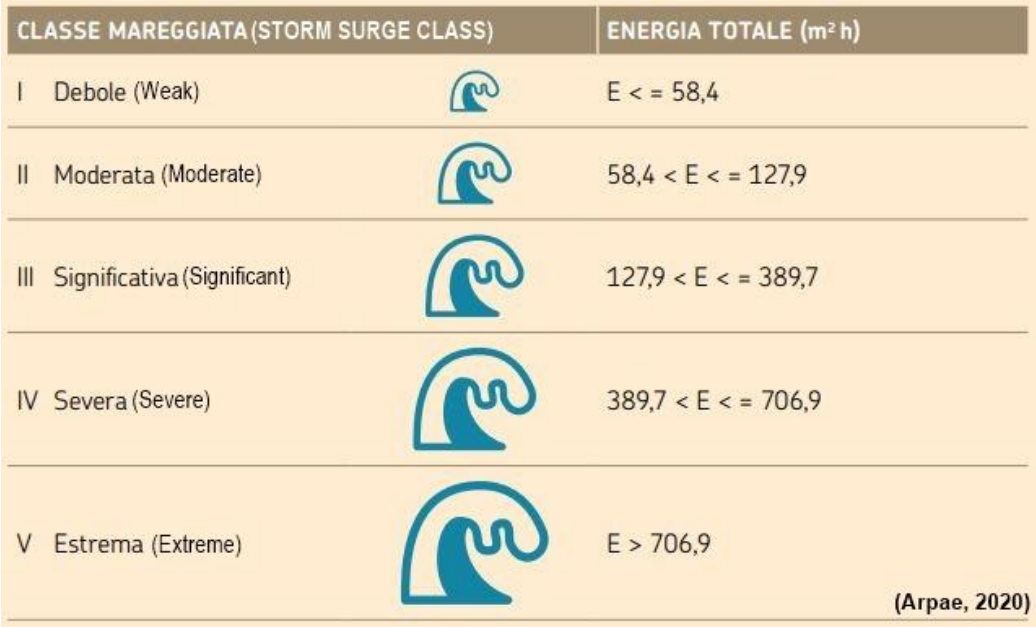

Figure 30. Storm surge classes based on the Arpae 2020 hydro-meteo and climate report.

Chapter 4. Discussion

4.1. DEM validation

There is a significant difference between the DEM and GPS elevation values in the back dune area in both October 2018 (Figure 14) and October 2019 (Figure 16) transects. There are two possibilities that can account for the elevation differences. The first one could be due to human error during the GPS survey as the pole can be dragged a few centimeters from the ground. Possible variance between in beach surfaces, systematic collection inconsistencies related to survey set-up and susceptibility to external factors such as possible digging of the pole and wind speed influence may be encountered on beach environments surveys (Talavera et al., 2018; Casella et al., 2020; Hilgendorf et al., 2021). Another possible cause is the misclassification of vegetation points to ground points that may have affected the surface reconstruction in the SfM processing. It can be recalled that the ground points were identified using the default parameters (maximum angle, maximum distance, cell size, and erosion radius) of the automatic classification process. This is to ensure standardization in the SfM processing and to reduce as much human bias as possible.

The model fitting statistics of the November 2020 (Figure 18) and October 2021 (Figure 20) datasets show a good fit (R^2 range of 0.83 – 0.99 for 2020 and 0.96 – 0.99 for 2021) between the DEM and GPS elevation values for most of the sample transects. There is still a slight shift of values in the back dune, which may also be caused by the issues specified above for the 2018 and 2019 datasets.

4.2. GCD, transect profile comparison, and vegetation change – 2021 vs 2016

The GCD result of the 2021 versus 2016 (Figure 21 and Figure 23) highlights a significant deposition – in terms of area, average depth, and volume, along the dune foot and portion of the beach. A total area of 2,221 m^2 erosion and 3,799 m^2 deposition was calculated, with an average depth of 0.17 m and 0.24 m, respectively. This translates to a total volume of 584 m^3 erosion and 1,109 m^3 of deposition that represents 34% and 66% of the thresholded values (Table 4).

The sand deposition along the fence has reduced the slope steepness and led to the increase in dune width. Progradation of around 3 to 5 m from the foredune has

been evident and that some profiles exhibit embryo dune development (Figure 23c, d, f, g, h, i, j). Embryo or insipient foredunes are formed due to sand deposition within relatively clumps of vegetation, individual plants, or driftwood/ log debris (Hesp, 2002; van Puijenbroek et al., 2016). Increase in driftwood and vegetation has been evident within and near the fence (Figure 26), along with the increase in sand deposition. The increase in vegetation colonization has contributed to the stabilization of sand accumulation within the dunes over 5 years, which was also evident in the study of van Puijenbroek et al. (2016). The result is also in agreement with the published work of Dong et al. (2008) and Hesp (2002), where it was mentioned that the establishment of vegetation on bare sand or beach forms a roughness element that may allow localized sand deposition and reduced erosion.

Profiles of transect 2, 3, 8, and 9 have the highest change both in terms of sand accumulation or embryo dune formation (Figure 23) and increase in vegetation (Figure 24 and Table 9), while transect 1 and 10 have exhibited erosional patterns in the beach area (Figure 23) and with lesser vegetation increase (5.2% and 7%, respectively). This can be accounted to the profile location since the transects with the highest positive change are within the middle part, while transects 1 and 10 are located along the two ends of the dune fence, with lesser protection against wind. Dune growth behind the fence was also evident in the study of Itzkin et al. (2009). Blowout patterns are also observed in the back dune at the end portions of the fence. However, these appear to be caused by misclassified points instead of actual blowouts as verified in the profile comparison and orthomosaic images of 2021 and 2016. Total vegetation removal in areas that are sparsely covered with grass or shrubs is particularly challenging in the SfM processing, so significant errors in bare earth elevation models are possible (Niethammer et al., 2012; Solazzo et al., 2018).

The overall foredune stoss slope has reduced given the sediment accumulation and the formation of insipient dunes within the fence. As the foredune stoss slope is supplied with sediment, it will grow seawards and upwards as insipient dunes may eventually become an established foredune (Saunders and Davidson-Arnott, 1990; Hesp, 2002).

No significant increase in the foredune heights have been observed in the profiles transects (Figure 23). Similar findings have been observed in the study of Itzkin

et al. (2009), where new insipient dunes are created seaward of the original dune following the emplacement of sand fences, but this have impeded the natural foredune from receiving additional sediment.

An erosional pattern is evident in the northern beach portion towards the northern head of the structure (Figure 21), which can be accounted for by the wind and wave trends in the area within the period of 2016 to 2021. Based on the wave direction (Figure 27a), the Bora storm surge may have eroded the northern end of the fence since both the wind and wave direction, during the analyzed time period, has been mainly coming from the Northeast (NE). Only February 2016 and November 2019 have wave direction coming from the Southeast or the Sirocco wind. The wave pattern from the Arpae report also agrees with the ERA5 data. The moderate storm surge record in 2017 (95.9 m^2h), 2018 (111.4 m^2h), and 2020 (76.3 m^2h) (Table 10) may have caused erosional changes in the area.

4.3. Annual change detection and error analysis

Assessment of the annual geomorphological changes were only possible for the GCD results of March 2017 versus October 2016 (Figure *31*a), November 2020 versus October 2019 (Figure 32b), and October 2021 versus November 2020 (Figure 32c). The GCD values referred in this section are in Table 5, Table 6, Table 7,Table 8 and the GCD maps are in the Appendix.

In the March 2017 versus October 2016 result, a total area of 781.86 m^2 erosion and 2,882 m^2 deposition was observed. In terms of volumetric change, there is a 120.52 m^3 of erosion and 708.86 m^3 of deposition, which accounts to 15% and 85% of the thresholded area of interest. Depositional patterns with vertical average depth of 0.25 m along the middle portion of the fence and the beach area were observed (Figure *31*a). There is a noticeable sand formation along the dune foot, which both the fence and the aeolian processes may have induced. This is supported by the study of Itzkin et al. (2020) where it was mentioned that the wind velocity decrease through dune fences would lead to a decrease in the shear stress acting on the bed; therefore, deposition in the lee side of the fence is expected. Supporting evidence suggest that within this period, winds from the ENE, E, and ESE directions have been prevalent (Figure 29a), which could have induced sediment deposition along the beach. Erosional patterns with vertical average depth of 0.15 m were observed at the northern head of

the structure – along the back dune and the beach. The erosional pattern on the back dune could be due to inaccuracy in point cloud classification process as previously mentioned, while the one in the beach may reflect erosion caused by the moderate storm surges within this period (Table 10) and the observed peak in SWH of about 1.1 m that was recorded in January 2017 (Figure 27b).

The results of the July 2017 versus March 2017 (Figure 31b), October 2018 versus July 2017 (Figure 31c), and October 2019 versus October 2018 (Figure 32a) produced erroneous GCD models due to DEM quality problem of the July 2017 and October 2018 data. Therefore, the GCD models that utilized these data are not representative of the annual geomorphic change in those periods. The SfM processing reports of these surveys were thoroughly examined to determine the possible source of the inaccuracies. The error source in the modelling was the GCP quality (Table 15). In the July 2017 SfM processing, the coordinates of the eight (8) pole corners (Figure 33a), which were surveyed in 2021, were used as a proxy data since the original GCPs were no longer available. The issue on the October 2018 data was the lack of original and well-spread GCP targets (Figure 33b). In the October 2019 versus October 2018 (Figure 32a), valid change detection patterns are discernable on the northern half of the study area wherein targets are in place. A depositional pattern of about 0.20 m to 0.60 m in depth is formed along the fence, while erosion of about 0.20 m to 0.60 m in depth is still evident on the northern end of the beach. Erosional pattern is also observed near the fence where driftwoods or log debris are usually situated. The driftwoods movement might have been affected by the moderate storm surge in 2018. Disregarding the southern portion with erroneous result, it is consistent with the previous pattern in 2017 – 2016 DEM differencing.

In the November 2020 versus October 2019 GCD, there is a total erosion area of 529.43 m^2 and 2,014.18 m^2 of deposition extent. A volume of 165.61 m^3 erosion and 523 m^3 of deposition was observed, which constitute to 24% and 76% of the thresholded area, respectively. Consistent with the previous results, it still shows depositional patterns with an average depth of 0.26 m within the fence (Figure 32b). However, sediment deposition of about 0.20 m to 0.70 m in depth is observed on the northern end of the beach instead of erosion. There is an apparent erosional pattern of about 0.20 m to 0.60 m in depth at the northern head of the structure, where driftwoods

typically accumulate close to the fence. The moderate storm surges from 2019 to 2020 may have again caused this shift given that a maximum SWH of 2.10 m and 3.11 m for 2019 and 2020 have been recorded.

The GCD result of the October 2021 versus November 2020 did not show much depositional change within the fence (Figure 32c), which can signify that the accumulated sediment is beginning to stabilize. As mentioned in the study of Eichmanns et al. (2021), the downwind sediment accumulation is one of the positive impacts of dune fencing that initiates dune stability. A total area of 2,382 m^2 has erosion and only 303.63 m^2 of the area has deposition. This translates to 705.04 m^3 of erosional and 73.87 m^3 of depositional volume, which represents 91% and 9% of the thresholded values. Wide erosional patterns are observed along the beach area, which could be due to aeolian influence given that the highest wind speed of 3.3 ms^{-1} over the course of 5 years was recorded in May 2021 based on the ERA5 data (Figure 28a). The high beach dynamics is expected since strong wind swells tend to roll around this period.

In summary, the results of the annual and the whole period change (2021-2016) show coherence in terms of the increase in sediment supply along the dune fence. Both erosional and depositional patterns have been obvious along the beach where driftwoods and the waterline are located, indicating the very high beach dynamics in the area. Erosion has been mainly observed within the beach, specifically on the northern end of the structure that can be explained by the influencing Bora wave and winds.

Precision issues with the SfM-derived DEM and GPS have been encountered due to target data quality and systemic issues as already discussed. Drone-based topographic reconstructions of beach environments tend to exhibit higher inaccuracies compared to other environments such as outcrops due to the low texture and contrast of sand surface, making photogrammetric methods, such as features matching, difficult (Eltner et al., 2015; Casella et al., 2020). Notwithstanding, the results in this study show that assessing the spatio-temporal evolution of the erosional and depositional processes in the Bevano dune ridge is possible using multi-temporal drone data. Elevation model accuracy in the order of ~5 to 8 cm has been achieved in all the surveys with sufficient and well-spread GCPs.

Chapter 5. Conclusions and recommendations

This thesis aimed to contribute to the assessment of the dune restoration project in the protected natural area of the Bevano River mouth in Ravenna (Italy), using UAV monitoring surveys from 2016 to 2021. The overall goal of the thesis was attained, and all the research objectives were met. Detailed geomorphic change detection analyses were presented using the proposed SfM and DEM differencing approach. A systematic workflow for UAV data processing that is suitable for sediment volume calculation was established. Applying a uniform and systematic workflow to SfM photogrammetry was important to identify and reduce errors in elevation modeling. Orthomosaic images for vegetation change detection was used as a supplemental tool to assess other contributing factors to the overall morphology of the study area.

Seasonal change, wind and waves contributed greatly to the annual erosion and deposition dynamics in the area. Progressive dune development also depends on weather and uninterrupted sequences of years without heavy storms. Despite the natural factors affecting the overall deposition dynamics, it can be concluded that the dune fencing proved to be an effective intervention to prevent dune erosion since significant geomorphological changes and vegetation colonization occurred in the 2021-2016 interval time. Main sand accumulation was observed along the dune foot where the wood fences were established. In addition, the following changes have also been observed – progradation of the front dune, development of insipient dunes, decrease in slope stoss, decrease of blowout features due to increase in vegetation colonization. Also, an increase in vegetation and debris cover within and near the wood fences were highlighted.

Regarding data elaboration, the Geomorphic Change Detection (GCD) toolset showed to be an effective monitoring tool for coastal dunes. However, sources of uncertainties or errors should be properly considered to improve the overall accuracy of the DEM differencing result. Recommendations regarding the UAV survey, SfM processing, and GCD modeling have to be taken into consideration in the future works to contribute to the continuous progress and workflow improvement for dune morphodynamics. First, consistency in the camera parameters for the UAV survey must be ensured to minimize model errors in the processing phase. DEMs can be further

improved by tweaking its build parameters such as the binning and spatial resolution. Another recommendation is to implement manual ground point classification as an additional step in the automatic classification in the SfM processing. By doing so, the DEMs for the change detection part could have improved as well. Addition of other possible sources of error as input in the GCD modeling process can be explored instead of just using the total error values of the GCP control points. This may reduce potential inaccuracies in the final DEM differencing results. Inclusion of morphological units can also be implemented in the GCD modelling to improve the volume calculation and assessment.

Overall, in a coastal management perspective, the results of this thesis can supplement in showcasing the importance of implementing dune fencing and limiting debris cleaning as nature-based solutions to combat dune degradation along the coastal zones of Ravenna. The proposed systematic workflow in this research can also be explored in creating transferable guidelines to relevant stakeholders in implementing ICZM.

Bibliography

1. Aagaard, T., Davidson-Arnott, R., Greenwood, B., Nielsen, B., 2004. Sediment supply from shoreface to dunes: linking sediment transport measurements and long-term morphological evolution. Geomorphology 60, 205–224. https://doi.org/10.1016/j.geomorph.2003.08.002.
2. Agisoft LLC, 2021. Agisoft Metashape User Manual: Professional Edition, Version 1.7.
3. Airoldi, L., Ponti, M., Abbiati, M., 2016. Conservation challenges in human dominated seascapes: The harbour and coast of Ravenna, Regional Studies in Marine Science, Volume 8, Part 2, Pages 308-318, ISSN 2352-4855, https://doi.org/10.1016/j.rsma.2015.11.003.
4. Alonso, Alcantara-Carrio, J., Cabrera, L., 2002. Tourist resorts and their impact on beach erosion at sotavento59uerteventurarteventura, Spain. J. Coastal Research. 7, 1–7. https://doi.org/10.2112/1551-5036-36.sp1.1.
5. Amaroli, C., Ciavola, P., Perini, L., Calabrese, L., Lorito, S., Valentini, A., Masina, M., 2011. Critical storm thresholds for significant morphological changes and damage along the Emilia-Romagna coastline, Italy. Geomorphology 143-144, 34-51 http://dx.doi.org/10.1016/j.geomorph.2011.09.006.
6. Anderson, K., Westoby, M., James, M., 2019. Low-budget topographic surveying comes of age: Structure from motion photogrammetry in geography and the geosciences. Progress in Physical Geography: Earth and Environment, 43, 163–173. https://doi.org/10.1177/0309133319837454.
7. Anthony, E.J., Vanhee, S., Ruz, M.-H., 2007. An assessment of the impact of experimental brushwood fences on foredune sand accumulation based on digital elevation models. Ecological Engineering, 31, 41–46. https://doi.org/10.1016/j.ecoleng.2007.05.005.
8. Arens, S.M., Baas, A.C.W., Van Boxel, J.H., Kaleman, C., 2001. Influence of reed stem density on foredune development. Earth Surf. Process. Landf. 26, 1161–1176. https://doi.org/10.1002/esp.257.
9. ARPAE Emilia-Romagna, 2020. Rapporto IdroMeteoClima Emilia-Romagna: Dati 2020. Retrieved from https://www.arpae.it/it/temi-ambientali/meteo/report-meteo/rapporti-annuali on 05 May 2022.

10. Ashmore P., Church, M., 1998. Sediment transport and river morphology: a paradigm for study. International Gravel-Bed Rivers Workshop 4: 115-148.
11. Atkins, J.P., Burdon, D., Elliott, M., Gregory, A.J., 2011. Management of the marine environment: integrating ecosystem services and societal benefits with the DPSIR framework in a systems approach. Mar. Pollut. Bull. 62 (2) 215–226. https://doi.org/10.1016/j.marpolbul.2010.12.012.
12. Barnard, S., Elliot, M., 2015. The 10-tenets of adaptive management and sustainability: An holistic framework for understanding and managing the socio-ecological system, Environmental Science & Policy, Volume 51, 181-191, ISSN 1462-9011. https://doi.org/10.1016/j.envsci.2015.04.008
13. Bird, E. C., 2011. Coastal geomorphology: an introduction. John Wiley & Sons. ISBN: 978-0-470-51729-1.
14. Biolchi, L.G., Unguendoli, S., Bressan, L., Giambastiani, B.M.S., Valentini, A., 2022. Ensemble technique application to an XBeach-based coastal Early Warning System for the Northwest Adriatic Sea (Emilia-Romagna region, Italy), Coastal Engineering, Volume 173, 104081, ISSN 0378-3839, https://doi.org/10.1016/j.coastaleng.2022.104081.
15. Callaghan, D.P., Ranasinghe, R., Short, A., 2009. Quantifying the storm erosion hazard for coastal planning. Coast. Eng. 56, 90–93. https://doi.org/10.1016/j.coastaleng.2008.10.003.
16. Carter, R.W.G., Stone, G.W., 1989. Mechanisms associated with the erosion of sand dune cliffs, Magilligan, Northern Ireland. Earth Surf. Process. Landf. 14, 1–10. https://doi.org/10.1002/esp.3290140102.
17. Casella, E., Drechsel, J., Winter, C., Benninghoff, M., Rovere, A., 2020. Accuracy of sand beach topography surveying by drones and photogrammetry. Geo-Marine Letters, 40:255-268. https://doi.org/10.1007/s00367-020-00638-8.
18. Coastal Engineering Research Center (CERC), 1984. Shore Protection Manual, US Army Corps of Engineers. Ft. Belvoir, Virginia. Retrieved from https://luk.staff.ugm.ac.id/USACE/USACE-ShoreProtectionManual1.pdf on 10 March 2021.
19. Cohn, N., Ruggiero, P., de Vries, S., & Kaminsky, G. M., 2018. New insights on

coastal foredune growth: The relative contributions of marine and aeolian processes. Geophysical Research Letters, 45. https://doi.org/10.1029/2018GL077836.

20. Daley, W., Jones, C., Vegliante, G., Mootoo, T. and Terchunian, A.V., 2000. A blueprint for coastal management: the West Hampton dunes story. Shore and Beach, 68:25-29.
21. Davidson-Arnott, R., Bauer, B., & Houser, C., 2019. Introduction to coastal processes and geomorphology. Cambridge university press. ISBN 978-0-521-69671-5.
22. De Vriend, H.J., Van Koningsveld, M., 2012. Building with Nature: Thinking, Acting and Interacting Differently. Ecoshape, Dordrecht, The Netherlands, p. 39. ISBN 978-94-6190-957-2.
23. Dias, J. A., Ferreira, O., Matias, A., Vila, A. and Sa-Pires, C., 2003. Evaluation of soft protection techniques in barrier islands by monitoring programs: case studies from Ria Formosa (Algarve, Portugal). Journal of Coastal Research, SI35:117-131. http://www.jstor.org/stable/40928755.
24. Dong, Z., Luo, W., Qian, G., and Lu, P., 2008. Wind tunnel simulation of the three-dimensional airflow patterns around shrubs. J. Geophys. Res.-Earth, 113, F02016, https://doi.org/10.1029/2007JF000880.
25. Edelman, T., 1972. Dune erosion during storm conditions. In: Coastal Engineering 1972. American Society of Civil Engineers, New York, NY, pp. 1305–1311. https://doi.org/10.1061/9780872620490.073.
26. Eichmanns, C., Schüttrumpf, H., 2020. Investigating Changes in Aeolian Sediment Transport at Coastal Dunes and Sand Trapping Fences: A Field Study on the German Coast. JMSE, 8, 1012. https://doi.org/10.3390/jmse8121012.
27. Eichmanns, C., Lechthaler, S., Zander, W., Pérez, M.V., Blum, H., Thorenz, F., Schüttrumpf, H., 2021. Sand Trapping Fences as a Nature-Based Solution for Coastal Protection: An International Review with a Focus on Installations in Germany. Environments, 8, 135. https:// doi.org/10.3390/environments8120135.
28. Eichmanns, C., Schüttrumpf, H., 2021. Influence of Sand Trapping Fences on Dune Toe Growth and Its Relation with Potential Aeolian Sediment Transport. JMSE, 9, 850. https://doi.org/10.3390/jmse9080850.

29. Eltner, A., Kaiser, A., Castillo, C., Rock, G., Neugirg, F., Abellan, A., 2015. Image-based surface reconstruction in geomorphometry – merits, limits and developments of a promising tool for geoscientists. Earth Surf Dyn Discuss 1445–1508. https://doi.org/10.5194/esurfd-3-1445-2015.
30. Esteves, L.S., Brown, J.M., Williams, J.J., Lymbery, G., 2012. Quantifying thresholds for significant dune erosion along the Sefton coast Northwest England. Geomorphology 143–144, 52–61. https://doi.org/10.1016/j.geomorph.2011.02.029.
31. Esteves, L.S., 2014. Managed realignment: A viable long-term coastal management strategy? SpringerBriefs in Environmental Science. New York: Springer. ISBN: 978-94-017-9028-4.
32. Fabbri, S., Giambastiani, B.M.S., Sistilli, F., Scarelli, F., Gabbianelli, G., 2017. Geomorphological analysis and classification of foredune ridges based on Terrestrial Laser Scanning (TLS) technology. Geomorphology 295. 436–451. http://dx.doi.org/10.1016/j.geomorph.2017.08.003.
33. Fabbri, S., Grottoli, E., Armaroli, C., Ciavola, P., 2021. Using High-Spatial Resolution UAV-Derived Data to Evaluate Vegetation and Geomorphological Changes on a Dune Field Involved in a Restoration Endeavour. Remote Sensing, 13, 1987. https://doi.org/10.3390/rs13101987.
34. Fernández-Montblanc, T., Duo, E., Ciavola, P., 2020. Dune reconstruction and revegetation as a potential measure to decrease coastal erosion and flooding under extreme storm conditions, Ocean & Coastal Management, Volume 188, 105075, ISSN 0964-5691, https://doi.org/10.1016/j.ocecoaman.2019.105075.
35. Forbes, D.L., Parkes, G.S., Manson, G.K., Ketch, L.A., 2004. Storms and shoreline retreat in the southern Gulf of St. Lawrence. Mar. Geol. 210, 169–204. https://doi.org/10.1016/j.margeo.2004.05.009.
36. Garcia-Lozano, C., Pintó, J., Roig-Munar, FX., 2020. Set of indices to assess dune development and dune restoration potential in beach-dune systems on Mediterranean developed coasts. J Environmental Managem ent. Apr 1; 259:1 09754. doi: 10.1016/j.jenvman.2019.109754. Epub 2019 D ec 4. PMID: 32072949.

37. Giambastiani, B., Greggio, N., Sistilli, F., Fabbri, S., Scarelli, F., Candiago, S., Anfossi, G., Lipparini, C., Cantelli, L., Antonellini, M., Gabbianelli, G., 2016. RIGED-RA project – Restoration and management of Coastal Dunes in the Northern Adriatic Coast, Ravenna Area – Italy. World Multidisciplinary Earth Sciences Symposium (WMESS 2016). IOP Conference Series: Earth and Environmental Science 44 (2016) 052038. doi:10.1088/1755-1315/44/5/052038
38. Gopalakrishnan, S., Smith, M.D., Slott, J.M., Murray, A.B., 2011. The value of disappearing beaches: a hedonic pricing model with endogenous beach width. Journal of Environmental Economics and Management, Volume 61, Issue 3, Pages 297-310, ISSN 0095-0696, https://doi.org/10.1016/j.jeem.2010.09.003.
39. Harley, M.D., Valentini, A., Armaroli, C., Perini, L., Calabrese, L., Ciavola, P., 2016. Can an early-warning system help minimize the impacts of coastal storms? A case study of the 2012 Halloween storm, northern Italy. Nat. Hazards Earth Syst. Sci. 16, 209–222. https://doi.org/10.5194/nhess-16-209-2016.
40. Herrington, T.O., 2004. Dune and beach management plan for Dover township federation of beaches. Technical Report 2819, Davidson Laboratory, USA, pp. 20.
41. Hersbach, H., Bell, B., Berrisford, P., Biavati, G., Horányi, A., Muñoz Sabater, J., Nicolas, J., Peubey, C., Radu, R., Rozum, I., Schepers, D., Simmons, A., Soci, C., Dee, D., Thépaut, J-N., 2019. ERA5 monthly averaged data on single levels from 1979 to present. Copernicus Climate Change Service (C3S) Climate Data Store (CDS). (Accessed on < 03-MAY-2022 >), 10.24381/cds.f17050d7.
42. Hesp, P., 2002. Foredunes and blowouts: initiation, geomorphology and dynamics. Geomorphology 48: 245 – 268. DOI: 10.1016/S0169-555X(02)00184-8.
43. Hilgendorf, Z., Marvin, M.C., Turner, C., Walker, I.J., 2021. Assessing Geomorphic Change in Restored Coastal Dune Ecosystems Using a Multi-Platform Aerial Approach. Remote Sensing. 13, 354. DOI: https://doi.org/10.3390/rs13030354.
44. Hotta, S., Kraus, N.C., Horikawa, K., 1987. Function of sand fences in controlling windblown sand. Coastal Sediments 87. ASCE, New York, pp. 772–787.

45. IPCC, 2014. Climate Change 2014: Synthesis Report. Contribution of Working Groups I, II and III to the Fifth Assessment Report of the Intergovernmental Panel on Climate Change. Intergovernmental Panel on Climate Change, Geneva, Switzerland.
46. Itzkin, M.; Moore, L.J.; Ruggiero, P.; Hacker, S.D., 2020. The effect of sand fencing on the morphology of natural dune systems. Geomorphology, 352, 106995. DOI: https://doi.org/10.1016/j.geomorph.2019.106995.
47. Jackson, N. L., & Nordstrom, K. F., 2020. Trends in research on beaches and dunes on sandy shores, 1969–2019. Geomorphology, 366, [106737]. DOI: https://doi.org/10.1016/j.geomorph.2019.04.009.
48. James, M.R., Chandler, J.H., Eltner, A., Fraser, C., Miller, P.E., Mills, J.P., Noble, T., Robson, S.; Lane, S.N., 2019. Guidelines on the use of structure-from-motion photogrammetry in geomorphic research. Earth Surf. Process. Landforms, 44, 2081–2084, doi:10.1002/esp.4637.
49. Kasprak, A., Bransky, N.D., Sankey, J.B., Caster, J., Sankey, T.T., 2019. The effects of topographic surveying technique and data resolution on the detection and interpretation of geomorphic change, Geomorphology, Volume 333, Pages 1-15, ISSN 0169-555X, https://doi.org/10.1016/j.geomorph.2019.02.020.
50. Kato, T., 2016. Chapter 4 - Prediction of photovoltaic power generation output and network operation. Integration of Distributed Energy Resources in Power Systems, 2016, p.77-108. ISBN: 9780128032121; DOI: 10.1016/B978-0-12-803212-1.00004-0.
51. Labuz, T., Finkl, C.W., & Makowski, C. (eds.), 2015. Environmental Management and Governance: 323 Advances in Coastal and Marine Resources, Coastal Research Library 8, DOI 10.1007/978-3-319-06305-8_14, Springer International Publishing Switzerland.
52. Lane, S. N., Westaway, R. M., and Hicks, M., 2003. Estimation of erosion and deposition volumes in a large, gravel-bed, braided river using synoptic remote sensing. Earth Surface Processes and Landforms, 28, 249–271. https://doi.org/10.1002/esp.483.
53. Laporte-Fauret, Q., Castelle, B., Michalet, R., Marieu, V., Bujan, S., Rosebery, D., 2021. Morphological and ecological responses of a managed coastal sand dune

to experimental notches, Science of The Total Environment, Volume 782, 2021, 146813, ISSN 0048-9697, https://doi.org/10.1016/j.scitotenv.2021.146813.

54. Lazarus, E.D., McNamara, D.E., Smith, M.D., Gopalakrishnan, S., Murray, A.B., 2011. Emergent behavior in a coupled economic and coastline model for beach nourishment. Nonlinear Process. Geophys. 18, 989–999. https://doi.org/10.5194/npg-18-989-2011.
55. Lee, S., Choi, C., Kim, J., 2012. Evaluating the suitability of the EGM2008 geopotential model for the Korean peninsula using parallel computing on a diskless cluster. Comput. Geosci. 2013; 52:132–145. DOI:10.1016/j.cageo.2012.09.017.
56. Livingstone, I., Wiggs, G.F., Weaver, C.M., 2007. Geomorphology of desert sand dunes: a review of recent progress. Earth Sci. Rev. 80 (3–4), 239–257. https://doi.org/10.1016/j.earscirev.2006.09.004.
57. Mancini, F., Dubbini, M., Gattelli, M., Stecchi, F., Fabbri, S., Gabbianelli, G., 2013. Using Unmanned Aerial Vehicles (UAV) for High-Resolution Reconstruction of Topography: The Structure from Motion Approach on Coastal Environments. Remote Sensing. 2013; 5(12):6880-6898. https://doi.org/10.3390/rs5126880.
58. Martinez, M.L., Gallego-Fernandez, J.B., Garcia-Franco, J.G., Moctezuma, C. and Jimenez, C.D., 2006. Assessment of coastal dune vulnerability to natural and anthropogenic disturbances along the Gulf of Mexico. Environmental Conser vation, 33:0 9-117. doi:10.1017/S0376892906002876.
59. Martínez, M.L., Psuty, N.P., Lubke, R.A., 2008. A Perspective on Coastal Dunes. In Coastal Dunes; Martínez, M.L., Psuty, N.P., Eds.; Ecological Studies; Springer: Berlin/Heidelberg, Germany, Volume 171, pp. 3–10. ISBN 978-3-540-74001-8.
60. Mascarenhas, A., 2009. An Experiment to Restore Coastal Sand Dunes at Miramar Beach, Goa: An Appraisal. Natural Resources of Goa: A Geological Perspective. Geological Society of Goa. ISBN 978-81-908737-0-3.
61. Matias, A., Ferreira, O., Mendes, I., Dias, J.A., Vila-Consejo, A., 2005. Artificial construction of dunes in the south of Portugal. J. Coast. Res. 21, 472–481. DOI: https://doi.org/10.2112/03-0047.1.
62. Maun, M. A., 2009. The biology of coastal sand dunes. Oxford University Press. doi: 10.1093/aob/mcp136.

63. Mendelssohn, I.A., Hester, M.W., Monteferrante, F.J. and Talbot, F., 1991. Experimental dune building and vegetative stabilization in a sand deficient barrier island setting on the Louisiana coast, USA. Journal Coastal Research, 7:37-149. DOI: http://www.jstor.org/stable/4297810.
64. Miller, D.L., Thetford, M., Yager, L., 2001. Evaluation of sand fence and vegetation for dune building following overwash by Hurricane Opal on Santa Rosa Island, Florida. J. Coast. Res. 17, 936–948. DOI: https://www.jstor.org/stable/4300253.
65. Murray, A.B., Gopalakrishnan, S., McNamara, D., Smith, M.D., 2013. Progress in coupling models of human and coastal landscape change. Comput. Geosci. 53, 30–33. https://doi.org/10.1016/j.cageo.2011.10.010.
66. Niethammer, U., James, M.R., Rothmund, S., Travelletti, J., Joswig, M. 2012. UAV-based remote sensing of the Super-Sauze landslide: Evaluation and results, Engineering Geology, Volume 128, Pages 2-11. ISSN 0013-7952. DOI: https://doi.org/10.1016/j.enggeo.2011.03.012.
67. Nordstrom, K.F., Arens, S.M., 1998. The role of human actions in evolution and management of foredunes in the Netherlands and New Jersey, USA. Journal of Conservation 4, 169–180. DOI: https://www.jstor.org/stable/25098280.
68. Nordstrom, K.F., 2008. Beach and Dune Restoration. Cambridge University Press, Cambridge. ISBN: 9780511535925. DOI: https://doi.org/10.1017/CBO9780511535925.
69. NSW Department of Land and Water Conservation, 2001. Coastal Dune Management: A Manual of Coastal Dune Management and Rehabilitation Techniques, Coastal Unit, DLWC, Newcastle. ISBN 0 7347 5202 4.
70. Overton, M.F., Pratikto, W.A., Lu, J.C., Fisher, J.S., 1994. Laboratory investigation of dune erosion as a function of sand grain size and dune density. Coast. Eng. 23, 151–165. DOI: https://doi.org/10.1016/0378-3839(94)90020-5.
71. Passalacqua P, Belmont P, Staley D, Simley J, Arrowsmith JR, Bode C, Crosby C, DeLong S, Glenn N, Kelly S, Lague D, Sangireddy H, Schaffrath K, Tarboton D,Wasklewicz T, Wheaton J., 2015. Analyzing high resolution topography for advancing the understanding of mass and energy transfer through landscapes. Earth-Science Reviews 148:174–193. DOI:

https://doi.org/1016/j.earscirev.2015.05.012.

72. Pilkey, O.H., Neal, W.J., Kelley, J.T., Cooper, J.A.G., 2011. The World's Beaches. University of California Press, Singapore. ISBN: 9780520268722.
73. Rozé, F. and Lemauviel, S., 2004. Sand Dune Restoration in North Brittany, France: A 10-Year Monitoring Study. Restoration Ecology, 12:29-35. DOI:10.1111/j.1061-2971.2004.00264.x.
74. Ruz, M.H., Anthony, E.J., 2008. Sand trapping by brushwood fences on a beach-foredune contact: The primacy of the local sediment budget. Zeit Geo Supp. 52, 179–194. DOI: 10.1127/0372-8854/2008/0052S3-0179.
75. Sallenger, A.H., 2000. Storm impact scale for barrier islands. J. Coast. Res. 16, 890–895. DOI: https://www.jstor.org/stable/4300099.
76. Sankey, J.B., Kasprak, A., and Caster, J., 2016. Geomorphic Process from Topographic Form: Automating the Interpretation of Repeat Survey Data to Understand Sediment Connectivity for Source-Bordering Aeolian Dunefields in River Valleys. Vol. 2016. DOI: https://doi.org/10.1002/esp.4143.
77. Sardá, R., Valls, J. F., & Pintó, J., 2013. Un nuevo modelo integral de gestión de playas. Un nuevo modelo integral de gestión de playas, 167-182. ISBN 978-84-9984-204-2.
78. Saunders, K.E., Davidson-Arnott, R.G.D., 1990. Coastal dune response to natural disturbances. Proc. Symposium on Coastal Sand Dunes. NRC, Ottawa, pp. 321 – 345.
79. Savage, R.P., 1963. Experimental study of dune building with sand fences. Proceedings of the 8th International Conference on Coastal Engineering, Mexico City, Mexico, ASCE, pp. 380–396. Retrieved from on 10 March 2022. https://icce-ojs-tamu.tdl.org/icce/index.php/icce/article/download/2271/1962
80. Scarelli, F.M., Sistilli, F., Fabbri, S., Cantelli, L., Barboza, E.G., Gabbianelli, G., 2017. Seasonal dune and beach monitoring using photogrammetry from UAV surveys to apply in the ICZM on the Ravenna coast (Emilia-Romagna, Italy), Remote Sensing Applications: Society and Environment, Volume 7, 2017, Pages 27-39, ISSN 2352-9385, https://doi.org/10.1016/j.rsase.2017.06.003.
81. Sekovski, I., Del Río, L., Armaroli, C., 2020. Development of a coastal vulnerability index using analytical hierarchy process and application to

Ravenna province (Italy), Ocean & Coastal Management, Volume 183, 2020, 104982, ISSN 0964-5691, https://doi.org/10.1016/j.ocecoaman.2019.104982.

82. Signell, R.P., Chiggiato, J., Horstmann, J., Doyle, J.D., Pullen, J., Askari, F., 2010. Highresolution mapping of Bora winds in the northern Adriatic Sea using Synthetic Aperture Radar. Journal of Geophysical Research 115, C04020. doi:10.1029/2009JC005524.
83. Silvestri, S., Nguyen Ngoc, D., Chiapponi, E., 2022. Comment on "Soil salinity assessment by using near-infrared channel and Vegetation Soil Salinity Index derived from Landsat 8 OLI data: a case study in the Tra Vinh Province, Mekong Delta, Vietnam" by Kim-Anh Nguyen, Yuei-An Liou, Ha-Phuong Tran, Phi-Phung Hoang and Thanh-Hung Nguyen. Progress in Earth and Planetary Science. Accepted.
84. Sloss, C. R., Shepherd, M. & Hesp, P., 2012. Coastal Dunes: Geomorphology. Nature Education Knowledge 3(10):2.
85. Solazzo, D., Sankey, J., Sankey, T., Munson, S., 2018. Mapping and measuring aeolian sand dunes with photogrammetry and LiDAR from unmanned aerial vehicles (UAV) and multispectral satellite imagery on the Paria Plateau, AZ, USA. Geomorphology 319, 174-185.
DOI: https://doi.org/10.1016/j.geomorph.2018.07.023
86. Stockdon, H.F., Sallenger, A.H., Holman, R.A., Howd, P.A., 2007. A simple model for the spatially variable coastal response to hurricanes. Mar. Geol. 238, 1–20. https://doi.org/10.1016/j.margeo.2006.11.004.
87. Stout, J.E., Warren, A., Gill, T.E., 2009. Publication trends in aeolian research: an analysis of the Bibliography of Aeolian Research. Geomorphology 105 (1–2), 6–17. https://doi.org/10.1016/j.geomorph.2008.02.015.
88. Talavera, L., Del Río, L., Benavente, J., Barbero, L., López-Ramírez, J., 2018. UAS as tools for rapid detection of storm-induced morphodynamic changes at Camposoto beach, SW Spain, International Journal of Remote Sensing, 39:15-16, 5550-5567, DOI: 10.1080/01431161.2018.1471549
89. Taramelli, A., Di Matteo, L., Ciaoval, P., Guadagnano, F., Tolomei, C., 2015. Temporal evolution of patterns and processes related to subsidence of the

coastal area surrounding the Bevano River mouth (Northern –driatic) - Italy. Ocean & Coastal Management 108, 74e88. http://dx.doi.org/10.1016/j.ocecoaman.2014.06.021.

90. Taylor, E.B., Gibeaut, J.C., Yoskowitz, D.W., Starek, M.J., 2015. Assessment and monetary valuation of the storm protection function of beaches and foredunes on the Texas coast. J. Coast. Res. 315, 1205–1216. https://doi.org/10.2112/JCOASTRESD-14-00133.1.
91. Thomas, D.S., Wiggs, G.F., 2008. Aeolian system responses to global change: challenges of scale, process, and temporal integration. Earth Surf. Process. Landf. 33 (9), 1396–1418. https://doi.org/10.1002/esp.1719.
92. van de Graaff, J., 1977. Dune erosion during a storm surge. Coast. Eng. 1, 99–134. https://doi.org/10.1016/0378-3839(77)90010-2.
93. Van der Biest, K.; De Nocker, L.; Provoost, S.; Boerema, A.; States, J.; Meire, P., 2017. Dune dynamics safeguard ecosystem services. Ocean & Coastal Management 149. 148-158. https://doi.org/10.1016/j.ocecoaman.2017.10.005.
94. Van Puijenbroek, M., Limpens, J., De Groot, A., Riksen, M., Gleichman, M., Slim, P., van Dobben, H., Berendse, F. 2017. Embryo dune development drivers: beach morphology, growing season precipitation, and storms: Embryo Dune Development and Climate. Earth Surface Processes and Landforms. DOI: 10.1002/esp.4144.
95. Wheaton, J., 2008. Uncertainty in Morphological Sediment Budgeting of Rivers. Unpublished PhD Thesis, University of Southampton, Southampton, 412 pp. Retrieved from https://sites.google.com/a/joewheaton.org/www/Home/research/projects-1/morphological-sediment-budgeting/phdthesis on 09 June 2022.
96. Wheaton, J., Brasington, J., Darby, S., Sear, D., 2009a. Accounting for uncertainty in DEMs from repeat topographic surveys: improved sediment budgets. Earth Surface Processes and Landforms, Volume 35, Issue 2 p. 136-156. https://doi.org/10.1002/esp.1886.
97. Wheaton, J., Brasington, J., Darby, S., Merz, J., Pasternack, G., Sear, D., Vericat, D., 2009b. Linking geomorphic changes to salmonid habitat at a scale relevant

to fish. River Research and Applications, Volume 26, Issue 4, p. 469-486. https://doi.org/10.1002/rra.1305.

98. Wong, P.P., Losada, I.J., Gattuso, J.-P., Hinkel, J., Khattabi, A., McInnes, K.L., Saito, Y., Sallenger, A., 2014. Coastal systems and low-lying areas. In: Field, C.B., Barros, V.R., Dokken, D.J., Mach, K.J., Mastrandrea, M.D., Bilir, T.E., Chatterjee, M., Ebi, K.L., Estrada, Y.O., Genova, R.C., Girma, B., Kissel, E.S., Levy, A.N., MacCracken, S., Mastrandrea, P.R., White, L.L. (Eds.), Climate Change 2014: Impacts, Adaptation, and Vulnerability. Part A: Global and Sectoral Aspects. Contribution of Working Group II to the Fifth Assessment Report of the Intergovernmental Panel on Climate Change. Cambridge University Press, Cambridge, United Kingdom and New York, NY, USA, pp. 361–409.
99. Wootton, L., Miller, J., Miller, C., Peek, M., Williams, A., and Rowe, P., 2016. New Jersey Sea Grant Consortium Dune Manual retrieved from njseagrant.org/dunemanual [27 March 2022].
100. World Commission on Environment and Development, WCED, 1987. Our Common Future. Oxford University Press, Oxford, UK.
101. Yousefi Lalimi, F., Silvestri, S. Moore, L. J., & Marani, M, 2017. Coupled topographic and vegetation patterns in coastal dunes: Remote sensing observations and ecomorphodynamic implications, J. Geophys. Res. Biogeosciences., 122, 119–130, doi:10.1002/2016JG003540.
102. Zanuttigh, B., Angelelli, E., Bellotti, G., Romano, A., Krontira, Y., Troianos, D., Suffredini, R., Franceschi, G., Cantù, M., Airoldi, L., Zagonari, F., Taramelli, A., Filipponi, F., Jimenez, C., Evriviadou, M., Broszeit, S., 2015. Boosting blue growth in a mild sea: analysis of the synergies produced by a multi-purpose offshore installation in the Northern Adriatic, Italy. Sustainability 7, 6804–6853. http://dx.doi.org/10.3390/su7066804.
103. Zavatarelli, M., Raicich, F., Bregant, D., Russo, A., Artegiani, A., 1998. Climatological biogeochemical characteristics of the Adriatic Sea. J. Mar. Syst. 18, 227–263. http://dx.doi.org/10.1016/S0924-7963(98)00014-1.
104. Zheng, Z., Du, S., Taubenböck, H., Zhang, X., 2022. Remote sensing techniques in the investigation of aeolian sand dunes: A review of recent

advances, Remote Sensing of Environment, Volume 271, 112913, ISSN 0034-4257, https://doi.org/10.1016/j.rse.2022.112913.

Appendix

Alignment parameters	Values
Accuracy	High
Generic preselection	Yes
Reference preselection	Source
Key point limit	40,000
Key point limit per Mpx	1,000
Tie point limit	4,000
Exclude stationary tie points	Yes
Guided image matching	No
Adaptive camera model fitting	No

Table 11. Values used for the alignment parameters in the SfM photogrammetry.

Optimization parameters	Details
Parameters	f, b1, b2, cx, cy, k1-k3, p1, p2
Adaptive camera model fitting	No
Depth maps generation	**Details**
Quality	Ultra-High
Filtering mode	Mild
Max neighbors	40
Dense Point Cloud	**Details**
Point colors	3 bands, uint8

Table 12. Details and parameters for the optimization process, depth maps, and dense point cloud generation.

Ground points classification	Details
Max angle (°)	15
Max distance (m)	1
Cell size (m)	50

Table 13. Details and parameters for the automatic ground points classification.

DEM reconstruction	Details
Source data	Dense cloud
Tile size	256
Face count	Medium
Enable ghosting filter	No
Orthomosaic	**Details**
vertex colors	3 bands, uint8
Blending mode	Mosaic
Surface	DEM
Enable hole filling	Yes
Enable ghosting filter	No
System	**Details**
Software name	Agisoft Metashape Professional
Software version	1.7.4 build 12898
OS Windows	64 bit
RAM	15.92 GB
CPU	Intel™ C™TM) i7-8700 CPU @ 3.20GHz
GPU(s)	GeForce GTX 1050

Table 14. Details and parameters for the DEM reconstruction, orthomosaic creation, and system settings of the SfM photogrammetry software.

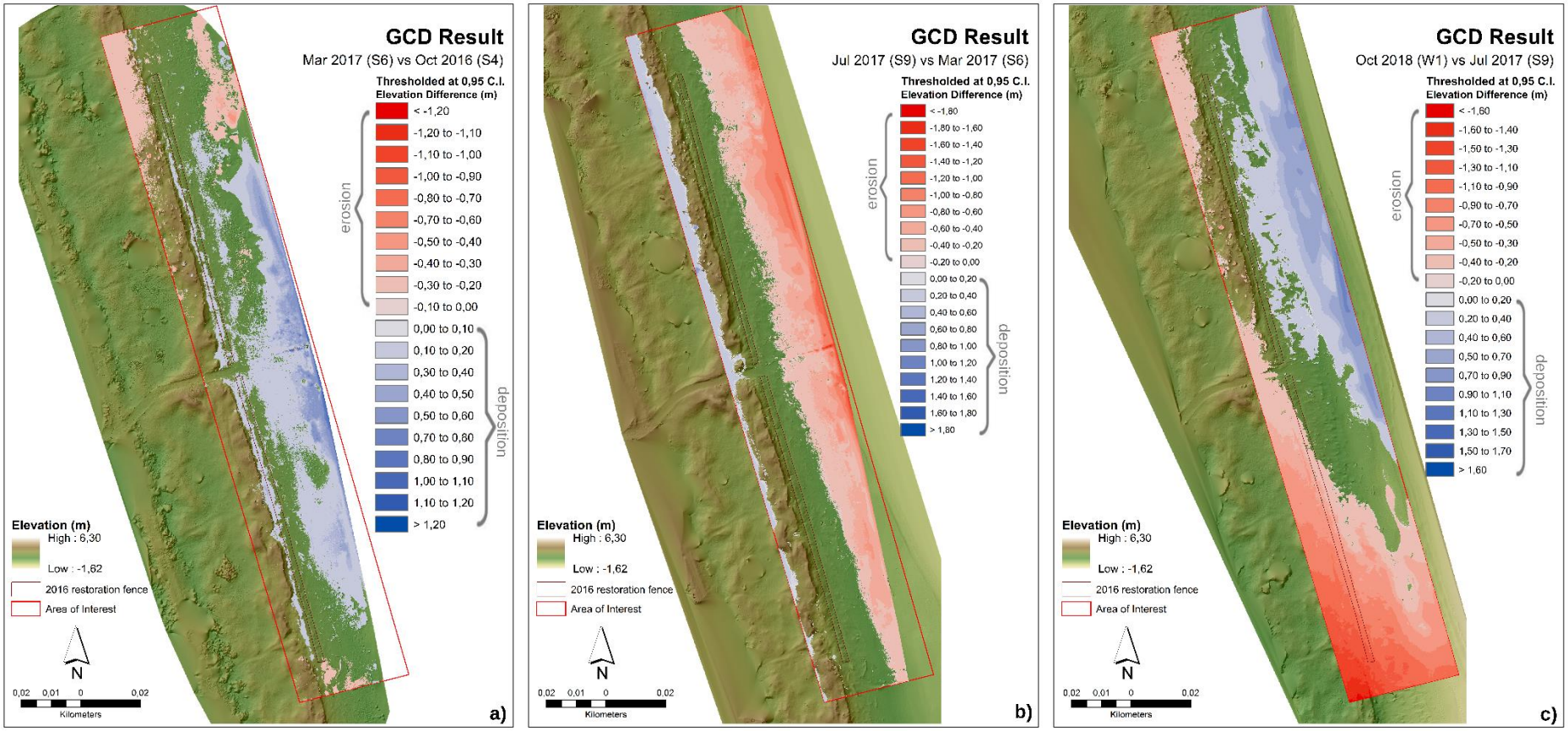

Figure 31. Annual change detection results – Mar 2017 vs Oct 2016 (a), Jul 2017 vs Mar 2017 (b), Oct 2018 vs Jul 2017 (c).

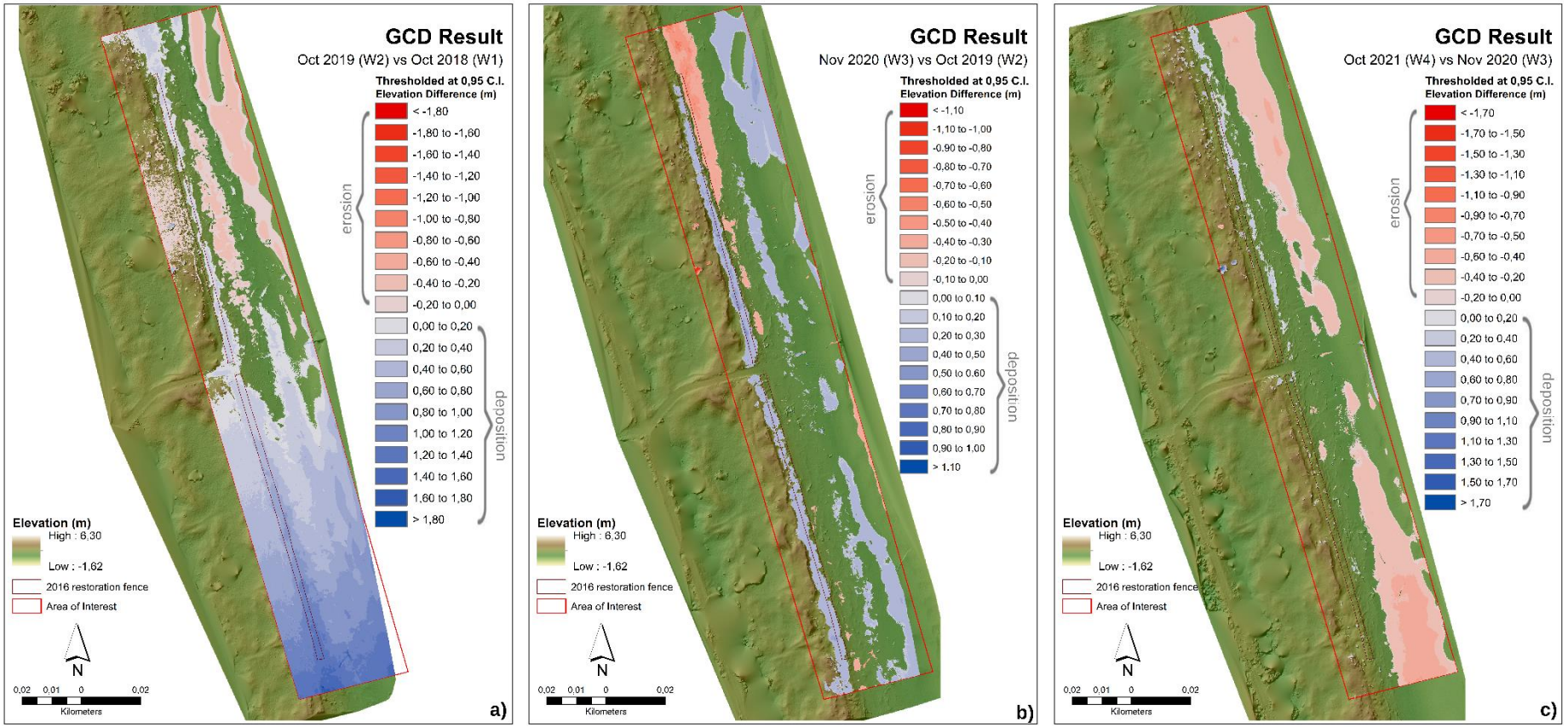

Figure 32. Annual change detection results – Oct 2019 vs Oct 2018 (a), Nov 2020 vs Oct 2019 (b), Oct 2021 vs Nov 2020 (c).

Survey dates	Number of targets (GCPs)	Remarks
28Oct2016 (S4)	13	well-distributed targets
08Mar2017 (S6)	15	
04Jul2017 (S9)	**8**	**pole corners from 2021 survey**
15Oct2018 (W1)	**9**	**only the northern part have targets**
30Oct2019 (W2)	12	well-distributed targets
05Nov2020 (W3)	12	additional targets from 2021 survey (poles) were added
25Oct2021 (W4)	15	well-distributed targets

Table 15. Survey details and the corresponding remarks in the error assessment.

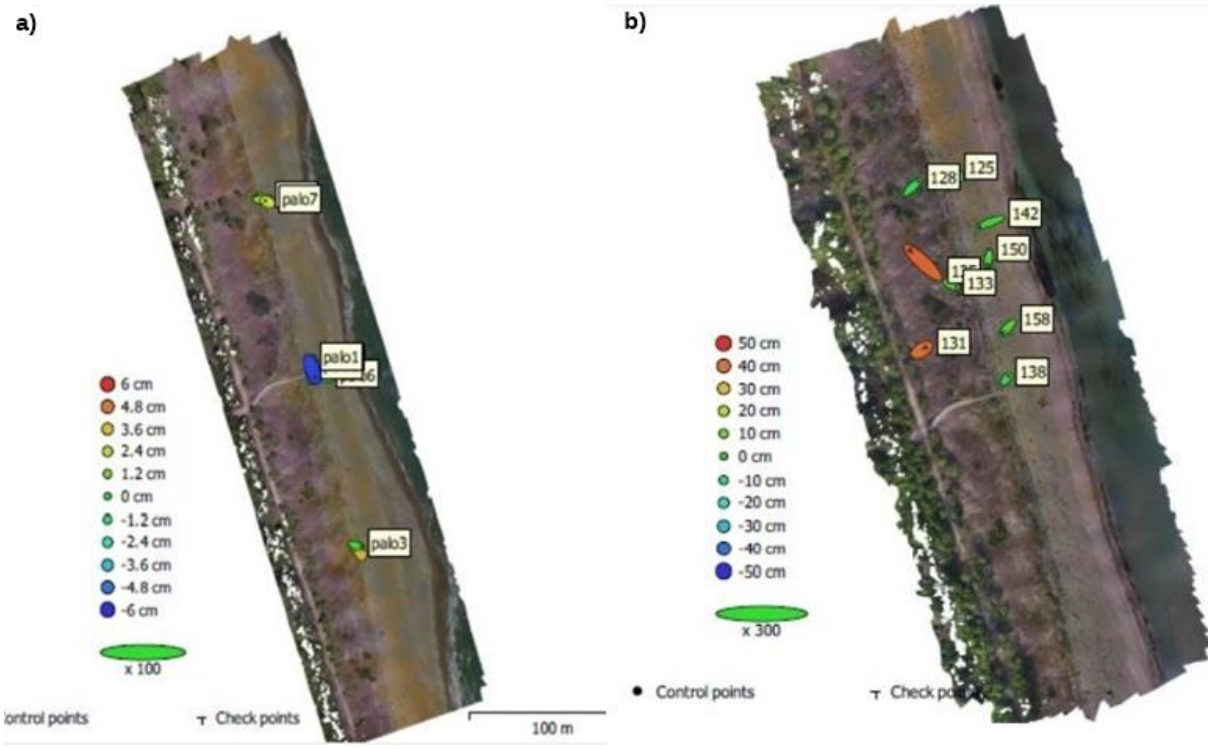

Figure 33. Location of the July 2017 (a) and Oct 2018 GCPs (b)